Electronic Supplementary Information

NO$_x$ production in a rotating gliding arc plasma: potential avenue for sustainable nitrogen fixation

Fatme Jardali,[a] Senne van Alphen, [a,b] James Creel,[a] Hamid Ahmadi Eshtehardi,[a,c] Magnus Axelsson,[d] Rune Ingels[d] Rony Snyders[b] and Annemie Bogaerts[a]

[a] Research group PLASMANT, Department of Chemistry, University of Antwerp, Universiteitsplein 1, BE-2610 Antwerp, Belgium.
[b] Research group ChIPS, Department of Chemistry, University of Mons, Av. Nicolas Copernic 3, 7000 Mons, Belgium.
[c] 4MAT , CP 165/63, Université Libre de Bruxelles, 50 Av. F.D. Roosevelt, B-1050 Brussels, Belgium
[d] N2 Applied, Beddingen 2, NO-0250 Oslo, Norway.

S.1. How ammonia from the manure is lost into the environment

When urea ($(NH_2)_2CO$) is applied to soil, the following reactions take place:

(i) Ammonium carbonate, an unstable compound, forms through the reaction $(NH_2)_2CO + H_2O \rightarrow (NH_4)_2CO_3$.

(ii) This compound quickly decomposes into NH_4^+ through $(NH_4)_2CO_3 + 2H^+ \rightarrow 2NH_4^+ + CO_2 + H_2O$, i.e., a reaction that consumes acidity.

(iii) Due to the high pH, volatile NH_3 gas is released through the reaction $NH_4^+ + OH^- \rightarrow NH_3 + H_2O$.[1]

Potential methods to reduce NH_3 volatilization include acidification of slurries, e.g. using sulphuric acid (H_2SO_4).[2] Consequently, by lowering the pH of the manure, NH_3 turns into NH_4^+, an involatile compound.[3] Alternatively, nitric acid (HNO_3) (or nitrate anion, NO_3^-, in its aqueous phase) can be used to convert volatile NH_3 into involatile ammonium nitrate (NH_4NO_3) through the reaction $NH_3 + HNO_3 \rightarrow NH_4NO_3$. HNO_3 can also readily be formed by dissolving NO_2 in water.

S.2. NO$_x$ concentrations and energy costs in various plasma types

Table S1. Reported values for NO$_x$ concentration and energy cost in various plasma types.

Plasma type	Concentration*	Energy cost	Ref.
Electric arc (Birkeland-Eyde)	2% NO	2.0 – 3.28 MJ mol^{-1} HNO$_3$	[4–6]
RF crossed discharge	-	24 - 108 MJ mol^{-1} HNO$_3$	[7]
Laser-produced plasma	-	8.9 MJ mol^{-1} NO$_x$	[8]
Pulsed corona discharge	-	186 MJ mol^{-1} HNO$_3$ 43 MJ mol^{-1} NO$_x$	[9,10]
(+/-) DC corona discharge	-	1057/1673 MJ mol^{-1} NO$_x$	[11]
(Pulsed)/Spark discharge	-	10 – 60 MJ mol^{-1} NO$_x$	[11–13]
Packed DBD	0.5% NO$_x$	18 MJ mol^{-1} NO$_x$	[14]
DBD	0.6% NO$_x$	56 – 140 MJ mol^{-1} NO$_x$	[15]
Pin-to-plane ns-pulsed spark discharge	-	5.0 – 7.7 MJ mol^{-1} NO$_x$	[15]
Pin-to-plane DC glow discharge	-	7 MJ mol^{-1} NO$_x$	[15]
Pin-to-pin DC glow discharge	0.7% NO$_x$	2.8 MJ mol^{-1} NO$_x$	[16]
DC plasma arc jet	6.5% NO	3.6 MJ mol^{-1} NO	[17]
Propeller arc	0.4% NO$_x$	4.2 MJ mol^{-1} NO$_x$	[15]
Pulsed milli-scale gliding arc	1-2% NO$_x$	2.8 - 4.8 MJ mol^{-1} NO$_x$	[18,19]
Gliding arc plasmatron	1.5% NO$_x$	3.6 MJ mol^{-1} NO$_x$	[20]
Microwave plasma	0.6% NO$_x$	3.76 MJ mol^{-1} NO$_x$	[21]
Microwave plasma with catalyst	6% NO	0.84 MJ mol^{-1} NO	[22]
Microwave plasma with magnetic field	14% NO	0.28 MJ mol^{-1} NO	[23]

* For certain plasma types, the NO$_x$ concentration is not reported.

S.3. Quantitative analysis of the products

The exhaust gas (comprising the product and unconverted feed gas) is analysed using a non-dispersive infra-red (NDIR) sensor, along with an ultra-violet sensor, for quantitative analysis of the species concentration (EMERSON Rosemount X-STREAM Enhanced XEGP continuous Gas Analyzer). The X-STREAM system is configured with four gases, two of which were used for this work: NO and NO$_2$. Exhaust gas from the RGA was input into the system at a flow rate of 500 mL/min through the use of a Bronkhorst mass flow controller; the specific flow rate of 500 mL/min was used as the system needed an input flow rate range between 50 mL/min and 1.5 L/min, although the choice of flow rate had no effect on the concentrations. The X-STREAM system was calibrated at the factory for NO$_2$ (UV sensor) and NO (NDIR sensor), and the calibration was again checked before measurements of the exhaust gas components, using known NO$_x$ concentrations from 1% to 8%.

We focus on measuring the NO and NO$_2$ concentrations and we report the total concentration as the sum of these two concentrations. This is due to the fact that NO$_2$ is the compound which is used in nitrogen fertilizer technology, as described in Section S.1 and the main article's Introduction section, and due to the tendency of NO to quickly oxidize into NO$_2$.

S.4. Raw experimental data

Table S2. Total flow rate and operating current applied, as well as the average power and average concentration of NO and NO$_2$ measured for each gas composition, for a rotating arc in Mode I.

Gas composition [N$_2$% / O$_2$%]	Total flow rate [L/min]	Current [mA]	Average power [W]	Concentration [%]		Energy cost [MJ mol^{-1}]
				NO	NO$_2$	
				Measurement 1		
20 / 80	2	70	111.91	0.51	2.13	3.05
40 / 60	2	70	111.72	0.69	2.65	2.41
50 /50	2	70	110.48	0.79	2.15	2.71
60 / 40	2	70	109.17	0.92	2.42	2.35
70 / 30	2	70	108.61	1.06	1.99	2.56
80 /20	2	70	105.84	1.17	1.31	3.07
				Measurement 2		
20 / 80	2	70	111.15	0.53	2.17	2.96
40 / 60	2	70	111.03	0.69	2.68	2.37
50 /50	2	70	111.10	0.80	2.65	2.32
60 / 40	2	70	109.64	0.91	2.34	2.43
70 / 30	2	70	107.62	1.06	1.97	2.56
80 /20	2	70	103.94	1.18	1.31	3.01
				Measurement 3		
20 / 80	2	70	110.61	0.54	2.17	2.94
40 / 60	2	70	110.10	0.70	2.65	2.37
50 /50	2	70	109.89	0.81	2.61	2.31
60 / 40	2	70	109.58	0.93	2.40	2.37
70 / 30	2	70	108.18	1.07	1.99	2.55
80 /20	2	70	105.13	1.20	1.31	3.02

Table S3. Total flow rate and operating current applied, as well as the average power and average concentration of NO and NO$_2$ measured for each gas composition, for a steady arc in Mode II.

Gas composition [N$_2$% / O$_2$%]	Total flow rate [L/min]	Current [mA]	Average power [W]	Concentration [%]		Energy cost [MJ mol^{-1}]
				NO	NO$_2$	
				Measurement 1		
20 / 80	2	149	222.81	0.61	4.13	3.45
40 / 60	2	137	203.04	0.78	4.59	2.72
50 /50	2	127	195.76	0.92	4.48	2.61
60 / 40	2	118	179.96	1.10	4.13	2.48
70 / 30	2	115	194.53	1.30	3.55	2.89
80 /20	2	117	167.14	1.55	2.50	2.97
				Measurement 2		
20 / 80	2	135	237.45	0.61	4.12	3.61
40 / 60	2	147	218.19	0.78	4.68	2.88
50 /50	2	131	201.11	0.93	4.66	2.59
60 / 40	2	122	182.06	1.10	4.08	2.53
70 / 30	2	119	174.36	1.32	3.58	2.56
80 /20	2	122	192.96	1.58	2.59	3.33
				Measurement 3		
20 / 80	2	138	227.76	0.61	3.99	3.56
40 / 60	2	144	215.60	0.81	4.68	2.83
50 /50	2	125	196.55	0.94	4.49	2.61
60 / 40	2	122	181.48	1.11	4.09	2.51
70 / 30	2	121	176.11	1.35	3.56	2.58
80 /20	2	122	164.91	1.59	2.53	2.88

S.5. Gas flow model

The gas flow behaviour in the reactor is characterized by a turbulent gas flow model (Reynolds-averaged-Navier-Stokes (RANS) model) within COMSOL Multiphysics®.[24] The following Navier-Stokes equations are solved for the mass and momentum conservation:

$$\nabla.(\rho \vec{u}_g) = 0 \tag{1}$$

$$\rho(\vec{u}_g.\nabla)\vec{u}_g = \nabla.\left[-p\vec{I} + (\mu + \mu_T)(\nabla \vec{u}_g + \nabla(\vec{u}_g)^T) - \frac{2}{3}(\mu + \mu_T)(\nabla.\vec{u}_g)\vec{I} - \frac{2}{3}\rho k_T\vec{I}\right] + \vec{F} \tag{2}$$

where ρ is for the gas density, $\vec{u}_g$ is the gas flow velocity vector, superscript T stands for transposition, p is the gas pressure, μ is the dynamic viscosity and μ_T is the turbulent viscosity of the fluid, k_T is the turbulent kinetic energy, $\vec{I}$ is the unity tensor and $\vec{F}$ is the body force vector.

The turbulence description follows the so-called Menter's Shear Stress Transport (SST) model, which uses the common k-ε model in the free stream and combines it with the more accurate k-ω model near the walls where the flow is more complicated.[25] This approach includes the following equations for the turbulent kinetic energy, k, and the specific dissipation, ω:

$$\rho(\vec{u}_g.\nabla)k = \nabla \cdot \left[(\mu + \mu_T\sigma_k)\nabla k\right] + P - \beta_0\rho\omega k \tag{3}$$

$$\rho(\vec{u}_g.\nabla)\omega = \nabla \cdot \left[(\mu + \mu_T\sigma_\omega)\nabla \omega\right] + \frac{\gamma}{\mu_T}\rho P - \beta_0\rho\omega^2 + 2(1 - f_{v1})\frac{\sigma_{\omega 2}\rho}{\omega}\nabla k \cdot \nabla \omega \tag{4}$$

where σ_k, σ_ω and γ are model coefficients defined in Equation 12, 13 and 14, and β_0 and $\sigma_{\omega 2}$ are dimensionless model constants defined in Table S4. The other symbols are explained below.

In Equation 1 and 2, μ_T is the turbulent viscosity of the fluid and is defined as:

$$\mu_T = \frac{a_1 k}{max(a_1\omega, Sf_{v2})} \tag{5}$$

where S is the absolute strain rate and a_1 is a dimensionless model constant defined in Table S4.

In Equation 4 and 5, f_{v1} and f_{v2} are two blending functions that control the switch from the k-ω model to the k-ε model in the free stream (where f_{v1} = 1):

$$f_{v1} = \tanh\left(\min\left(\theta_2^2, \frac{4\sigma_{\omega 2}k}{CD_{k\omega}y^2}\right)\right)^4 \tag{6}$$

$$f_{v2} = \tanh\left(\theta_2^2\right) \tag{7}$$

where y is the y-component of the position vector, and θ_2 and $CD_{k\omega}$ are placeholders for the following terms:

$$CD_{k\omega} = max\left(2\rho\sigma_{\omega 2}\frac{1}{\omega}\frac{\partial k}{\partial x}\frac{\partial \omega}{\partial x}, 10^{-10}\right) \tag{8}$$

$$\theta_2 = max\left(\frac{2\sqrt{k}}{\beta_0\omega l_W^2}, \frac{500\mu}{y^2\omega}\right) \tag{9}$$

where l_W is the wall distance.

In Equation 4, P serves as a product limiter coefficient and is defined as:

$$P = \min\left(P_k 10\rho\beta_0 k\omega\right) \tag{10}$$

where P_k is a placeholder for the following term:

$$P_k = \mu_T\left(\nabla\vec{u}_g : \left(\nabla\vec{u}_g + (\nabla\vec{u}_g)^T\right) - \frac{2}{3}\cdot(\nabla\cdot\vec{u}_g)^2\right) - \frac{2}{3}\rho k\nabla\cdot\vec{u}_g \tag{11}$$

The model coefficients in Equation 3 and 4 are defined as:

$$\sigma_k = f_{v1}\cdot\sigma_{k1} + (1 - f_{v1})\sigma_{k2} \tag{12}$$

$$\sigma_\omega = f_{v1}\cdot\sigma_{\omega1} + (1 - f_{v1})\sigma_{\omega2} \tag{13}$$

$$\gamma = f_{v1}\cdot\gamma_1 + (1 - f_{v1})\gamma_2 \tag{14}$$

σ_{k1}, σ_{k2}, $\sigma_{\omega1}$, $\sigma_{\omega2}$, γ_1 and γ_2 are dimensionless model constants defined in Table S4.

Table S4. Dimensionless model constants used in the SST turbulent flow model.

Model constant	Value
σ_{k1}	0.85
σ_{k2}	1
$\sigma_{\omega1}$	0.5
$\sigma_{\omega2}$	0.856
γ_1	0.5556
γ_2	0.44
a_1	0.31
β_0	0.09

S.6. Circuit of the 3D thermal plasma model

The gas breakdown and the arc formation between cathode and anode wall is simulated by solving a current conservation equation based on Ohm's law, using the electric potential, V, and the electric conductivity, σ, as dependent variables.

$$\nabla\cdot J = 0 \tag{15}$$

$$J = \sigma E \tag{16}$$

$$E = -\nabla V \tag{17}$$

Here, J is the current density and E the electric field. Figure S1 represents a scheme of the electrical circuit used in the model. The cathode is connected to a ballast resistor which in turn is connected to a voltage source supplying 3 kV, and the anode wall is grounded. The current is limited by a 200 Ω ballast resistor (Rb), and a 10 pF capacitor (Cb) forms an RC filtering circuit. The total current for the system is varied by changing the value for the ballast resistor.
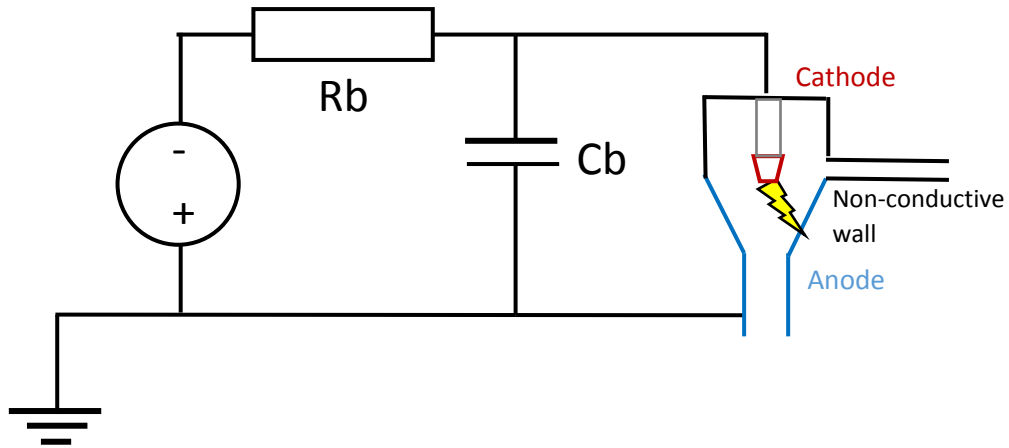
Figure S1. Scheme of the electrical circuit used for the RGA reactor in the model.

S.7. 3D thermal plasma model

The heat equation for the gas thermal balance is:

$$\rho C_p \frac{\partial T_g}{\partial t} + \rho C_p \vec{u}_g \cdot \nabla T_g - \nabla \cdot (k_g \nabla T_g) = Q \tag{18}$$

where ρ is the gas density, C_p is the gas heat capacity at constant pressure, k_g is the gas thermal conductivity, T_g is the gas temperature and Q the heat source term, which includes Ohmic heating (due to the electric current) and radiation loss. The heat transfer equation is coupled to the turbulent gas flow model through the gas flow velocity, $\vec{u}_g$.

S.8. Gas properties of the 3D turbulent flow model and thermal plasma model

The material properties used in the 3D turbulent flow model and the thermal plasma model are adopted from the COMSOL 5.5 materials database for air.[24] The temperature dependencies of these properties are considered by interpolation of the property values listed in Table S3. In this table, T is the temperature, ρ is the gas density, C_p is the heat capacity at constant pressure, μ is the dynamic viscosity, k is the thermal conductivity, and σ is the electrical conductivity.

Table S5. Temperature dependency of the properties considered in the 3D turbulent flow model and thermal plasma model.

T [K]	ρ [kg m³]	c_p [J kg⁻¹ K⁻¹]	μ [pa s]	k [W m⁻¹ K⁻¹)	σ (S m⁻¹)
500	0,702	1047,30	0,0000271	0,041	0,000
600	0,585	1069,40	0,0000308	0,048	0,000
700	0,501	1086,30	0,0000344	0,055	0,000
800	0,439	1102,80	0,0000379	0,062	0,000
900	0,390	1119,00	0,0000412	0,068	0,000
1000	0,351	1135,00	0,0000445	0,075	0,000
1100	0,319	1150,90	0,0000476	0,081	0,000
1200	0,293	1167,00	0,0000507	0,088	0,000
1300	0,270	1183,60	0,0000537	0,094	0,000
1400	0,251	1200,70	0,0000566	0,101	0,000
1500	0,234	1218,50	0,0000595	0,107	0,000
1600	0,219	1237,20	0,0000624	0,114	0,000
1700	0,207	1256,90	0,0000652	0,121	0,000
1800	0,195	1278,00	0,0000679	0,128	0,000
1900	0,185	1301,40	0,0000706	0,136	0,000
2000	0,176	1328,40	0,0000733	0,145	0,000
2100	0,167	1361,10	0,0000759	0,155	0,000
2200	0,159	1402,50	0,0000786	0,168	0,000
2300	0,152	1456,30	0,0000812	0,183	0,000
2400	0,146	1527,20	0,0000837	0,203	0,000
2500	0,140	1620,40	0,0000863	0,228	0,000
2600	0,134	1741,20	0,0000888	0,260	0,000
2700	0,129	1894,40	0,0000914	0,301	0,001
2800	0,124	2083,50	0,0000939	0,350	0,002
2900	0,119	2309,50	0,0000965	0,407	0,004
3000	0,114	2569,40	0,0000990	0,472	0,009
3100	0,110	2854,80	0,0001017	0,542	0,036
3200	0,105	3150,80	0,0001043	0,610	0,064
3300	0,101	3435,10	0,0001070	0,672	0,110
3400	0,097	3679,00	0,0001097	0,719	0,182
3500	0,093	3851,90	0,0001125	0,746	0,290
3600	0,089	3927,30	0,0001152	0,750	0,444
3700	0,086	3891,30	0,0001179	0,731	0,662
3800	0,082	3749,70	0,0001205	0,693	0,958
3900	0,079	3527,80	0,0001231	0,646	1,351
4000	0,076	3263,60	0,0001257	0,598	1,861
4100	0,074	2996,60	0,0001282	0,555	2,510
4200	0,072	2757,90	0,0001307	0,522	3,325
4300	0,070	2566,80	0,0001331	0,501	4,332
4400	0,068	2431,50	0,0001356	0,493	5,563
4500	0,066	2353,20	0,0001379	0,497	7,051
4600	0,064	2329,50	0,0001403	0,515	8,831
4700	0,063	2357,10	0,0001426	0,544	10,942
4800	0,061	2433,10	0,0001450	0,587	13,426
4900	0,060	2555,80	0,0001473	0,642	16,325

5000	0,058	2724,50	0,0001496	0,711	19,684
5100	0,057	2939,80	0,0001519	0,794	23,551
5200	0,056	3202,40	0,0001543	0,892	27,976
5300	0,054	3514,50	0,0001566	1,006	33,011
5400	0,053	3818,00	0,0001589	1,137	38,712
5500	0,052	4294,80	0,0001612	1,286	45,108
5600	0,050	4766,70	0,0001636	1,452	52,304
5700	0,049	5294,80	0,0001660	1,636	60,352
5800	0,048	5879,50	0,0001683	1,837	69,280
5900	0,046	6519,60	0,0001707	2,053	79,181
6000	0,045	7212,10	0,0001731	2,283	90,194
6100	0,043	7951,60	0,0001755	2,522	102,390
6200	0,042	8729,70	0,0001778	2,767	115,900
6300	0,041	9534,20	0,0001802	3,011	130,860
6400	0,039	10349,00	0,0001825	3,248	147,460
6500	0,038	11153,00	0,0001848	3,471	165,910
6600	0,037	11921,00	0,0001870	3,670	186,490
6700	0,035	12624,00	0,0001892	3,837	209,480
6800	0,034	13230,00	0,0001913	3,963	235,230
6900	0,033	13707,00	0,0001933	4,043	264,100
7000	0,032	14026,00	0,0001952	4,070	296,470
7100	0,030	14164,00	0,0001970	4,043	332,690
7200	0,029	14108,00	0,0001988	3,964	373,050
7300	0,028	13859,00	0,0002005	3,837	417,770
7400	0,027	13428,00	0,0002021	3,670	467,000
7500	0,027	12842,00	0,0002037	3,473	520,760
7600	0,026	12134,00	0,0002053	3,256	579,030
7700	0,025	11344,00	0,0002069	3,031	641,670
7800	0,024	10513,00	0,0002086	2,806	708,530
7900	0,024	9678,30	0,0002102	2,591	779,370
8000	0,023	8870,60	0,0002119	2,390	853,990
8100	0,023	8113,30	0,0002136	2,208	932,120
8200	0,022	7425,50	0,0002153	2,046	1013,500
8300	0,022	6806,30	0,0002171	1,907	1098,000
8400	0,022	6268,20	0,0002189	1,788	1185,200
8500	0,021	5807,30	0,0002207	1,690	1275,000
8600	0,021	5427,50	0,0002225	1,611	1367,300
8700	0,020	5102,50	0,0002243	1,550	1461,700
8800	0,020	4856,60	0,0002261	1,504	1558,200
8900	0,020	4647,40	0,0002279	1,471	1656,500
9000	0,020	4497,30	0,0002297	1,451	1756,400
9100	0,019	4408,00	0,0002315	1,443	1857,800
9200	0,019	4327,30	0,0002332	1,443	1960,500
9300	0,019	4318,40	0,0002349	1,454	2064,400
9400	0,019	4302,30	0,0002366	1,471	2169,300
9500	0,018	4352,70	0,0002382	1,497	2275,200
9600	0,018	4418,00	0,0002398	1,529	2381,800
9700	0,018	4463,10	0,0002413	1,565	2489,100
9800	0,018	4605,40	0,0002421	1,609	2597,100
9900	0,017	4688,60	0,0002441	1,656	2705,500
10000	0,017	4867,20	0,0002453	1,709	2814,200

S.9.   2D Non-thermal plasma model

A quasi-neutral plasma, in which the electron and total ion densities are equal at all times, is assumed in the 2D plasma model.

This is achieved by calculating the density of one ion ($n_{NO_2^-}$) by balancing the electron density (n_e) with the densities of the other ions ($n_{N_2^+}, n_{O_2^+}, n_{NO^+}$) :

$$n_{NO_2^-} = \left(n_{N_2^+} + n_{O_2^+} + n_{NO^+} - n_e \right) \tag{19}$$

The model solves the following equation for the various neutral species, balancing the diffusion and convection of each plasma species with its production and loss rates due to chemical reactions:

$$\frac{\partial n}{\partial t} + \nabla(D\nabla n) + (\vec{u}_g.\nabla)n = R \tag{20}$$

where n is the species density, D is the diffusion coefficient, $\vec{u}_g$ the gas flow velocity vector and R the sum of all production and loss rates due to the chemical reactions.

For the ions, an extra ion mobility (μ_i) term is added to the above equation to account for their migration due to the ambipolar electric field ($\vec{E}_{amb}$):

$$\frac{\partial n_i}{\partial t} + \nabla\left(D_i\nabla n_i + \mu_i n_i \vec{E}_{amb}\right) + (\vec{u}_g.\nabla)n_i = R \tag{21}$$

For the electrons, the migration is calculated in the same way, using the electron mobility (μ_e):

$$\frac{\partial n_e}{\partial t} + \nabla\left(D_e\nabla n_e - \mu_e n_e \vec{E}_{amb}\right) + (\vec{u}_g.\nabla)n_e = R \tag{22}$$

The average electron energy $\bar{\varepsilon}_e$ is calculated through:

$$\frac{\partial n_e\bar{\varepsilon}_e}{\partial t} + \nabla.\left(-\mu_{\varepsilon,e}n_e\vec{E}_{amb} - D_{\varepsilon,e}\nabla\left(n_e\bar{\varepsilon}_e\right)\right) + (\vec{u}_g.\nabla)n_e\bar{\varepsilon}_e = q_e\vec{E}.\vec{G}_e + n_e\Delta\bar{\varepsilon}_e + Q_{bg} \tag{23}$$

where n_e is the electron density, q_e is the elementary charge, $\vec{E}$ the externally applied electric field, $\Delta\bar{\varepsilon}_e$ the energy exchanged in inelastic collisions with molecules, and Q_{bg} the background heat source serving as a stabilization term for the simulation. The terms $\mu_{\varepsilon,e}$ and $D_{\varepsilon,e}$ stand for the electron energy mobility and diffusion coefficient, respectively:

$$\mu_{\varepsilon,e} = \frac{5}{3}\mu_e \tag{24}$$

$$D_{\varepsilon,e} = \frac{2}{3}\mu_{\varepsilon,e}\bar{\varepsilon}_e \tag{25}$$

with μ_e the electron mobility. The electron flux $\vec{G}_e$ is derived from:

$$G_e = -D_e\nabla n_e - \mu_e n_e \vec{E}_{amb} \tag{26}$$

with D_e the electron diffusion coefficient. The ambipolar electric field $\vec{E}_{amb}$ is solved as follows:

$$\vec{E}_{amb} = \frac{\nabla n_i(-D_e + D_i)}{n_i(\mu_i + \mu_e)} \tag{27}$$

Finally, instead of the Poisson equation, the charge conservation equation is solved:

$$\nabla[\sigma_{pl}(-\nabla\varphi)] = 0 \tag{28}$$

where σ_{pl} stands for the plasma conductivity and φ stands for the electric potential.

$$\sigma_{pl} = |q_e|(\mu_e n_e + \mu_i n_i) \tag{29}$$

Solving this non-thermal plasma model in three dimensions, including the transport and reactions of all species in an N_2/O_2 plasma, would require an excessively long computation time. Therefore, the model is calculated for a 2D axisymmetric geometry with a limited chemical reaction set, as described in section S.12 below. Since this model correctly incorporates the heat terms of all plasma processes and reactions occurring in an N_2/O_2 plasma, the results from this 2D model can be used to correct the gas temperature of the 3D thermal model, as explained below.

S.10. Scaling of the 3D thermal plasma temperature

The calculated gas temperature of the thermal plasma model is scaled using the results of the axisymmetric 2D non-thermal plasma model that correctly incorporates the heat terms of all plasma processes and reactions occurring in an N_2/O_2 plasma. As the thermal model correctly describes the gas temperature gradients, the absolute values of the temperature are corrected using the following formula:

$$\frac{T - 293.15}{T_{factor}} + 293.15 \tag{30}$$

Here, T is the unscaled gas temperature, calculated by the 3D thermal plasma model and T_{factor} the correction factor to match T to the temperature of the 2D non-thermal plasma model, which was found to be 3.15. The original, or uncorrected, and the corrected temperature profiles, resulting from the 3D thermal plasma model, are shown in Figure S2.

<div align="center">(a)   (b)</div>
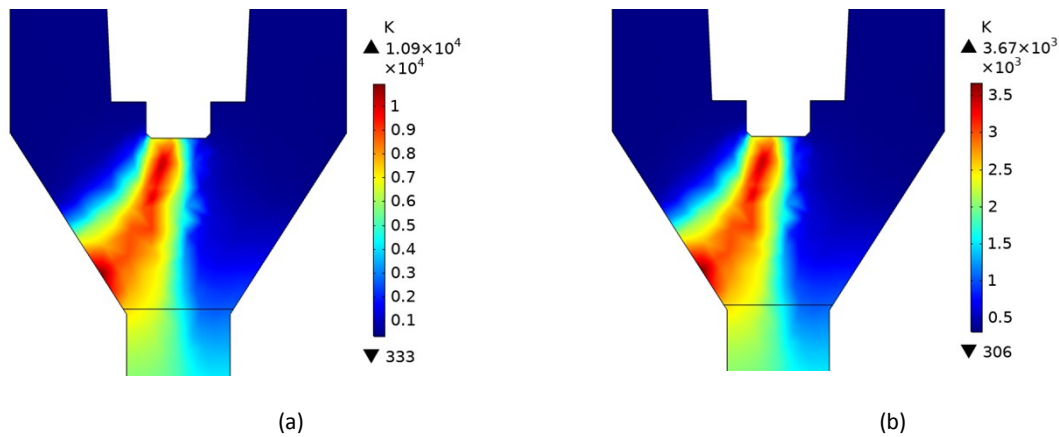
Figure S2. Original (i.e. uncorrected) (a) and corrected (b) temperature profiles of the thermal plasma model.

S.11. Chemical kinetics model

A chemical kinetics model is developed to calculate the NO_x concentration and to reveal the chemical pathways for NO_x formation in the RGA. The Zero-Dimensional Plasma Kinetics solver, ZDPlasKin,[26] is used to calculate the species number density by solving the continuity equation for the various species

$$\frac{dn_i}{dt} = \sum_r c_{r,i} k_r \prod_q n_q \qquad (31)$$

where $c_{r,i}$ is the stoichiometry number of species i in reaction r, k_r is the rate coefficient and q are the colliding species in reaction r. The rate coefficients of the heavy particle reactions are taken from literature and are a function of the gas or electron temperature, whereas the rate coefficients for the electron impact reactions are calculated using the electron impact cross sections and the electron energy distribution function (EEDF) through BOLSIG+,[27] coupled to ZDPlasKin. The electric field is provided as an input for the calculation of the EEDF which returns the mean electron energy at which the rate coefficients are evaluated.

The dissociation processes can result in an increase in the total number density of the species. Consequently, the pressure of the system will increase. In order to keep the pressure constant, we modify all species densities after each time progression to return to the desired pressure. This changes the mass density such that it is no longer the initial value. Therefore, for any calculation involving initial densities and new densities (after modification), the new densities are normalized to the initial value such that the mass density is the same. Both the modification and normalization are assumed linear, i.e. an equal multiplication factor is applied for all gas phase species.

S.12. Plasma chemistry included in the models

The full chemistry set used in the quasi-1D chemical kinetics model was recently developed and validated for a gliding arc plasmatron.[20] The chemistry set includes 81 different species, besides the electrons (see Table S6). These species react with each other in 1,214 electron impact reactions, 481 ionic reactions and 432 neutral reactions, as well as 2,478 vibration-vibration exchanges and vibration-translation relaxations between N_2 and O_2. A reduction in the chemistry set is crucial for higher dimensional modelling. Species included in the reduced set are represented in bold face in Table S6. Reducing the set is done by gradually removing species from the full set, and comparing the species densities obtained from the reduced model to those from the full model. This is done to ensure that the reduced set still properly describes the N_2/O_2 plasma chemistry. In addition, in this reduced set, the vibrational levels of N_2 and O_2 are considered as 1 lumped level which is further explained in section S.13.

Table S6. Species included in the model, besides the electrons. The symbol "V" followed by a number represents the vibrational level of the species under consideration. Species included in the reduced set are presented in bold face.

Neutral species	Radicals	Charged species	Excited species
N_2, O_2, **O_3,** **NO**, **NO_2**, N_2O, NO_3, N_2O_3, N_2O_4, N_2O_5	**N**, N(2D), N(2P), **O**, O(1D), O(1S)	N^+, N_2^+, N_3^+, N_4^+, O^-, O_2^-, O_3^-, O_4^-, O^+, O_2^+, O_4^+, **NO^+**, NO_2^+, N_2O^+, NO^-, **NO_2^-**, N_2O^-, NO_3^-, $O_2^+N_2$	**$N_2(V1-V24)$,** **$O_2(V1-V15)$,** $N_2(A^3\Sigma_u^+)$, $N_2(B^3\Pi_g)$, **$N_2(C^3\Pi_u)$**, **N_2** $(a'^1\Sigma_u^-)$, $O_2(a^1\Delta)$, $O_2(b^1\Sigma^+)$, **O_2** $(A^3\Sigma^+, C^3\Delta, c^1\Sigma^-)_a$

^{a} $O_2(A^3\Sigma^+, C^3\Delta, c^1\Sigma^-)$ is a combination of three electronic excited states with a threshold energy of 4.5 eV.

A list of all electron impact processes and their corresponding rate coefficients are presented in Table S7. Whenever the rate coefficient is not indicated, this implies that the reactions are treated by energy-dependent cross sections. When indicated, rate coefficients are expressed in $cm^3 s^{-1}$ or $cm^6 s^{-1}$ for binary or ternary reactions, respectively. The list includes vibrational excitation and de-excitation, electronic excitation and de-excitation, direct and dissociative ionization, dissociation, as well as direct and dissociative attachment reactions.

Table S7. Electron impact reactions implemented in the model for atomic and molecular nitrogen and oxygen species as well as NO$_x$ species.

Reaction	Rate coefficient	Ref.	Note	Reaction	Rate coefficient	Ref.	Note
$e + N_2 \leftrightarrow e + N_2($		28		$e + O_3 \rightarrow 2e + O +$		29	
$e + N_2(v) \leftrightarrow e + I$		28		$e + O_3 \rightarrow e + O$		30	
$e + N_2(g,v) \rightarrow e +$		31	a, b, c	$e + O_2(g,v) \rightarrow e +$		31	a
$e + N_2(E_x) \rightarrow e +$		31	b	$e + O_3 \rightarrow e + O_2 +$		29	
$e + N_2(g,v) \rightarrow 2e$		32	a	$e + O_2(g,v) \rightarrow O + ($		31	a, c
$e + N_2(E_x) \rightarrow 2e +$		32	b	$e + O_2(g,v) + M \rightarrow$		33	a, c, f
$e^- + N \rightarrow 2e^- + N^+$		34		$e + O_3 \rightarrow O + O_2$		32	
$e + N_2(g,v) \rightarrow 2e$		35	a	$e^- + O_3 \rightarrow O + O_2^-$		32	
$e + N_2(g,v) \rightarrow e +$		31	a, c	$e + O_3 + M \rightarrow O_3 +$	5×10^{-31}	36	f
$e + N_2(E_x) \rightarrow e + I$		31	b	$e^- + O + M \rightarrow O^- +$	1×10^{-31}	37	f
$e + N \rightarrow e + N(E_x$		31	d	$e^- + NO \rightarrow 2e^- +$		38	
$e + O_2 \leftrightarrow e + O_2($		28		$e + NO_2 \rightarrow 2e + I$		39	
$e + O_2(v) \leftrightarrow e + O$		40		$e + N_2O \rightarrow 2e +$		41	
$e + O_2(g,v) \rightarrow e +$		31	a, c, e	$e + N_2O \rightarrow e + N_2$		42	
$e + O_2(E_x) \rightarrow e +$		31	e	$e + N_2O \rightarrow e + N_2$		42	
$e + O_2(g,v) \rightarrow 2e$		32	a, c	$e + N_2O \rightarrow e + NO$		42	
$e + O_2(E_x) \rightarrow 2e +$		43	e	$e^- + NO \rightarrow O^- + N$		38	
$e^- + O \rightarrow 2e^- + O^+$		31		$e + N_2O \rightarrow N_2 + O$		41	
$e + O_2(g,v) \rightarrow 2e$		43	a, c	$e^- + NO_2 \rightarrow NO_2^-$	1×10^{-11}	44	
$e + O_2(E_x) \rightarrow 2e +$		43	e	$e + NO_2 \rightarrow O + NO$	1×10^{-11}	45	
				$e^- + NO + M \rightarrow NO^-$	8×10^{-31}	45	f
				$e + N_2O + M \rightarrow N_2O$	6×10^{-33}	45	f

a For any species indicated with (g,v), g and v stand for its ground and vibrationally excited state, respectively.
b $N_2(E_x)$ represents the electronically excited states: $N_2(A^3\Sigma_u^+)$, $N_2(B^3\Pi_g)$, $N_2(C^3\Pi_u)$ and $N_2(a^1\Sigma_u^-)$.
c The cross sections of the reactions involving excited species on the left hand side are shifted over the difference in the threshold energies.

d $N(E_x)$ represents the electronically excited states of atomic N: $N(2D)$ and $N(2P)$.

e $O_2(E_x)$ represents the electronically excited states: $O_2(a^1\Delta)$, $O_2(b^1\Sigma^+)$ and a combination of three states, i.e. $O_2(A^3\Sigma^+_u, C^3\Delta, c^1\Sigma^-)$ at a threshold energy of 4.5 eV.

f M represents any neutral species.

A list of all neutral-neutral reactions and their corresponding rate-coefficient expressions is presented in Table S8. The rate coefficients are expressed in $cm^3 s^{-1}$ or $cm^6 s^{-1}$ for binary or ternary reactions, respectively. For certain reactions, the rate coefficients of the vibrationally excited species are determined according to the Fridman-Macheret model in which the activation energy is lowered by αE_v, where α is the vibrational efficiency to lower the activation barrier and E_v is the vibrational energy. For those reactions, the α parameter is given in the last column of Table S8.

Table S8. Neutral-neutral reactions included in the model and the corresponding rate coefficient expressions. Tg is the gas temperature in K. The rate coefficients are expressed in $cm^3 s^{-1}$ or $cm^6 s^{-1}$ for binary or ternary reactions, respectively.

Reaction	Rate coefficient	Ref.	Note
$N_2(g,v) + M \rightarrow N + N + M$	$8.37 \times 10^{-4} \times \left(\frac{T_g}{298}\right)^{-3.5} \times \exp\left(-\frac{11371(}{T_g}\right)$	46	a, b $\alpha = 1$
$N + N + M \rightarrow N_2 + M$	$1.38 \times 10^{-33} \times \exp\left(\frac{502.978}{T_g}\right)$	47	b
$N + N \rightarrow N_2^+ + e^-$	$2.7 \times 10^{-11} \times \exp\left(-\frac{6.74 \times 10^4}{T_g}\right)$	45	
$N + N + N \rightarrow N_2(A^3\Sigma_u^+) + N$	1.0×10^{-32}	45	
$N + N + N \rightarrow N_2(B^3\Pi_g) + N$	1.4×10^{-32}	45	
$N + N + N_2 \rightarrow N_2(A^3\Sigma_u^+) + N_2$	1.7×10^{-33}	45	
$N + N + N_2 \rightarrow N_2(B^3\Pi_g) + N_2$	2.4×10^{-33}	45	
$N(2D) + M \rightarrow N + M$	2.4×10^{-14}	48	b
$N(2P) + N \rightarrow N(2D) + N$	1.8×10^{-12}	45	
$N(2P) + N_2 \rightarrow N + N_2$	2.0×10^{-18}	45	
$N_2(a^1\Sigma_u^-) + N \rightarrow N_2 + N$	2.0×10^{-11}	48	
$N_2(a^1\Sigma_u^-) + N_2 \rightarrow N_2 + N_2$	3.7×10^{-16}	48	
$N_2(a^1\Sigma_u^-) + N_2 \rightarrow N_2(B^3\Pi_g) + N_2$	1.9×10^{-13}	45	
$N_2(a^1\Sigma_u^-) + N_2(a^1\Sigma_u^-) \rightarrow N_2^+ + N_2 + e$	5.0×10^{-13}	48	
$N_2(a^1\Sigma_u^-) + N_2(a^1\Sigma_u^-) \rightarrow N_4^+ + e$	1.0×10^{-11}	45	
$N_2(a^1\Sigma_u^-) + N_2(A^3\Sigma_u^+) \rightarrow N_4^+ + e$	4.0×10^{-12}	45	
$N_2(A^3\Sigma_u^+) + N \rightarrow N_2 + N(2P)$	$4.0 \times 10^{-11} \times \left(\frac{300}{T_g}\right)^{0.667}$	45	
$N_2(A^3\Sigma_u^+) + N \rightarrow N_2 + N$	2.0×10^{-12}	45	
$N_2(A^3\Sigma_u^+) + N_2 \rightarrow N_2 + N_2$	3.0×10^{-16}	45	
$N_2(A^3\Sigma_u^+) + N_2(a^1\Sigma_u^-) \rightarrow N_2^+ + N_2 + e$	1.0×10^{-12}	48	
$N_2(A^3\Sigma_u^+) + N_2(A^3\Sigma_u^+) \rightarrow N_2 + N_2(A^3\Sigma_u^+)$	2.0×10^{-12}	48	
$N_2(A^3\Sigma_u^+) + N_2(A^3\Sigma_u^+) \rightarrow N_2 + N_2(B^3\Pi_g)$	3.0×10^{-10}	45	
$N_2(A^3\Sigma_u^+) + N_2(A^3\Sigma_u^+) \rightarrow N_2 + N_2(C^3\Pi_u)$	1.5×10^{-10}	45	
$N_2(B^3\Pi_g) + N_2 \rightarrow N_2 + N_2$	2.0×10^{-12}	45	
$N_2(B^3\Pi_g) + N_2 \rightarrow N_2(A^3\Sigma_u^+) + N_2$	3×10^{-11}	45	
$N_2(C^3\Pi_u) + N_2 \rightarrow N_2 + (a^1\Sigma_u^-)$	1.0×10^{-11}	45	
$O_2(g,v) + M \rightarrow O + O + M$	$\left(\frac{3.0 \times 10^{-6}}{T_g}\right) \times \exp\left(\frac{-59380}{T_g}\right)$		a $\alpha = 1$
$O + O + M \rightarrow O_2 + M$	$5.21 \times 10^{-35} \times \exp\left(\frac{900}{T_g}\right)$	49	b
$O + O_3 \rightarrow O_2 + O_2$	$8.0 \times 10^{-12} \times \exp\left(-\frac{2056}{T_g}\right)$	50	
$O + O_2(g,v) + M \rightarrow O_3 + M$	$1.34 \times 10^{-34} \times \left(\frac{T_g}{298}\right)^{-1.0}$	51	a, b

14

Reaction	Rate coefficient	Ref	Notes
$O_3 + M \rightarrow O_2 + O + M$	$7.16 \times 10^{-10} \times \exp\left(-\dfrac{98120}{R_g T_g}\right)$	52	b, c
$O + O_2(E_x) + M \rightarrow O_3 + M$	$1.34 \times 10^{-34} \times \left(\dfrac{T_g}{298}\right)^{-1.0}$	51	b, d, e
$O + O_3 \rightarrow O_2 + O_2(a^1\Delta)$	$2.0 \times 10^{-11} \times \exp\left(-\dfrac{2280}{T_g}\right)$	45	
$O_2(a^1\Delta) + O \rightarrow O_2 + O$	7.0×10^{-16}	45	
$O_2(a^1\Delta) + O_2 \rightarrow O_2 + O_2$	$3.8 \times 10^{-18} \times \exp\left(-\dfrac{205}{T_g}\right)$	45	
$O_2(b^1\Sigma^+) + O \rightarrow O_2(a^1\Delta) + O$	8.1×10^{-14}	45	
$O_2(b^1\Sigma^+) + O \rightarrow O_2 + O(1D)$	$3.4 \times 10^{-11} \times \left(\dfrac{T_g}{300}\right)^{-0.1} \times \exp\left(-\dfrac{4200}{T_g}\right)$	45	
$O_2(b^1\Sigma^+) + O_2 \rightarrow O_2 + O_2(a^1\Delta)$	$4.3 \times 10^{-22} \times (T_g)^{2.4} \times \exp\left(-\dfrac{281}{T_g}\right)$	45	
$O_2(b^1\Sigma^+) + O_3 \rightarrow O_2 + O_2 + O$	2.2×10^{-11}	45	
$O_2(a^1\Delta) + O_3 \rightarrow O_2 + O_2 + O(1D)$	$5.2 \times 10^{-11} \times \exp\left(-\dfrac{2840}{T_g}\right)$	45	
$O_2(a^1\Delta) + O_2(a^1\Delta) \rightarrow O_2 + O_2(b^1\Sigma^+)$	$7.0 \times 10^{-28} \times (T_g)^{3.8} \times \exp\left(\dfrac{700}{T_g}\right)$	45	
$O(1D) + O \rightarrow O + O$	8.0×10^{-12}	45	
$O(1D) + O_2 \rightarrow O + O_2$	$6.4 \times 10^{-12} \times \exp\left(-\dfrac{67}{T_g}\right)$	45	
$O(1S) + O \rightarrow O(1D) + O(1D)$	$5.0 \times 10^{-11} \times \exp\left(-\dfrac{300}{T_g}\right)$	45	
$O(1S) + O_2 \rightarrow O + O_2$	$1.3 \times 10^{-12} \times \exp\left(-\dfrac{850}{T_g}\right)$	45	
$O(1S) + O_2 \rightarrow O + O + O$	3.0×10^{-12}	45	
$O(1S) + O_2(a^1\Delta) \rightarrow O + O + O$	3.2×10^{-11}	45	
$O(1S) + O_2(a^1\Delta) \rightarrow O(1D) + O_2(b^1\Sigma^+)$	2.9×10^{-11}	45	
$O(1S) + O_2 \rightarrow O + O_2(A^3\Sigma^+, C^3\Delta, c^1\Sigma^-)$	$3.0 \times 10^{-12} \times \exp\left(-\dfrac{850}{T_g}\right)$	45	f
$N + O_2(g,v) \rightarrow O + NO$	$2.36 \times 10^{-11} \times \exp\left(-\dfrac{44230}{R_g T_g}\right)$	53	a, c $\alpha = 0.24$
$O + N_2(g,v) \rightarrow N + NO$	$3.01 \times 10^{-10} \times \exp\left(-\dfrac{318000}{R_g T_g}\right)$	54	a, c $\alpha = 1$
$O_3 + N \rightarrow NO + O_2$	$5.0 \times 10^{-12} \times \exp\left(-\dfrac{650}{T_g}\right)$	50	
$O_3 + NO \rightarrow O_2 + NO_2$	$2.5 \times 10^{-13} \times \exp\left(-\dfrac{765}{T_g}\right)$	45	
$O_3 + NO_2 \rightarrow O_2 + NO_3$	$1.2 \times 10^{-13} \times \exp\left(-\dfrac{2450}{T_g}\right)$	44	
$NO_3 + O_3 \rightarrow NO_2 + O_2 + O_2$	1.0×10^{-17}	55	
$N + NO \rightarrow O + N_2$	1.66×10^{-11}	56	
$N + NO_2 \rightarrow O + O + N_2$	9.1×10^{-13}	45	
$N + NO_2 \rightarrow O + N_2O$	3.0×10^{-12}	45	
$N + NO_2 \rightarrow N_2 + O_2$	7.0×10^{-13}	45	
$N + NO_2 \rightarrow NO + NO$	2.3×10^{-12}	45	
$O + NO \rightarrow N + O_2$	$7.5 \times 10^{-12} \times \left(\dfrac{T_g}{300}\right) \times \exp\left(-\dfrac{19500}{T_g}\right)$	45	

Reaction	Rate coefficient	Ref.	Notes
$O + NO_2 \rightarrow NO + O_2$	$9.05 \times 10^{-12} \times \left(\dfrac{T_g}{298}\right)^{-0.52}$	57	
$O + N_2O \rightarrow NO + NO$	$1.5 \times 10^{-10} \times \exp\left(-\dfrac{14090}{T_g}\right)$	45	
$O + N_2O \rightarrow N_2 + O_2$	$8.3 \times 10^{-12} \times \exp\left(-\dfrac{14000}{T_g}\right)$	45	
$O + NO_3 \rightarrow O_2 + N_2$	1.0×10^{-11}	45	
$NO + NO \rightarrow N + NO_2$	$3.3 \times 10^{-16} \times \left(\dfrac{300}{T_g}\right)^{0.5} \times \exp\left(-\dfrac{39200}{T_g}\right)$	45	
$NO + NO \rightarrow O + N_2O$	$2.2 \times 10^{-12} \times \exp\left(-\dfrac{32100}{T_g}\right)$	45	
$NO + NO \rightarrow N_2 + O_2$	$5.1 \times 10^{-13} \times \exp\left(-\dfrac{33660}{T_g}\right)$	45	
$NO + N_2O \rightarrow N_2 + NO_2$	$4.6 \times 10^{-10} \times \exp\left(-\dfrac{25170}{T_g}\right)$	45	
$NO + NO_3 \rightarrow NO_2 + NO_2$	1.7×10^{-11}	45	
$NO_2 + NO_2 \rightarrow NO + NO_3$	$4.5 \times 10^{-10} \times \exp\left(-\dfrac{18500}{T_g}\right)$	45	
$NO_2 + NO_2 \rightarrow NO + NO + O_2$	$3.3 \times 10^{-12} \times \exp\left(-\dfrac{13500}{T_g}\right)$	45	
$NO_2 + NO_3 \rightarrow NO + NO_2 + O_2$	$2.3 \times 10^{-13} \times \exp\left(-\dfrac{1600}{T_g}\right)$	45	
$NO_3 + NO_3 \rightarrow O_2 + NO_2 + NO_2$	$4.3 \times 10^{-12} \times \exp\left(-\dfrac{3850}{T_g}\right)$	45	
$NO + O_2(g,v) \rightarrow O + NO_2$	$2.8 \times 10^{-12} \times \exp\left(-\dfrac{23400}{T_g}\right)$	45	a $\alpha = 1$
$NO + NO + O_2(g,v) \rightarrow NO_2 + NO_2$	$3.3 \times 10^{-39} \times \exp\left(-\dfrac{4410}{R_g T_g}\right)$	58	a, c $\alpha = 0.2$
$NO_2 + O_2(g,v) \rightarrow NO + O_3$	$2.8 \times 10^{-12} \times \exp\left(-\dfrac{25400}{T_g}\right)$	45	a $\alpha = 0.2$
$NO_3 + O_2(g,v) \rightarrow O_3 + NO_2$	$1.5 \times 10^{-12} \times \exp\left(-\dfrac{15020}{T_g}\right)$	45	a $\alpha = 0.8$
$NO + O \rightarrow NO_2$	$3.01 \times 10^{-11} \times \left(\dfrac{T_g}{300}\right)^{-0.75}$	59	
$NO_2 + NO + M \rightarrow N_2O_3 + M$	$3.09 \times 10^{-34} \times \left(\dfrac{T_g}{300}\right)^{-7.70}$	50	b
$NO_2 + NO_2 + M \rightarrow N_2O_4 + M$	$1.4 \times 10^{-33} \times \left(\dfrac{T_g}{300}\right)^{-3.8}$	50	b
$NO_2 + NO_3 + M \rightarrow N_2O_5 + M$	$3.7 \times 10^{-30} \times \left(\dfrac{300}{T_g}\right)^{4.10}$	58	b
$N + O + M \rightarrow NO + M$	$1.0 \times 10^{-32} \times \left(\dfrac{300}{T_g}\right)^{0.5}$	45	b
$N_2(g,v) + O + M \rightarrow N_2O + M$	$3.9 \times 10^{-35} \times \exp\left(-\dfrac{10400}{T_g}\right)$	45	b
$N_2O + M \rightarrow N_2 + O + M$	$1.20 \times 10^{-9} \times \exp\left(-\dfrac{240000}{R_g T_g}\right)$	45	b, c

$NO_2 + M \rightarrow NO + O + M$	$9.4 \times 10^{-5} \times \left(\dfrac{T_g}{298}\right)^{-2.66} \times \exp\left(-\dfrac{31100(}{R_g T_g}\right)$	59	b, c
$NO_3 + M \rightarrow NO + O_2 + M$	$2.51 \times 10^{-14} \times \exp\left(-\dfrac{10230}{R_g T_g}\right)$	60	b, c
$NO + M \rightarrow N + O + M$	$8.7 \times 10^{-9} \times \exp\left(-\dfrac{75994}{T_g}\right)$	45	b
$N_2O_3 + M \rightarrow NO + NO_2 + M$	$1.91 \times 10^{-7} \times \left(\dfrac{T_g}{298}\right)^{-8.7} \times \exp\left(-\dfrac{40570}{R_g T_g}\right)$	50	b, c
$N_2O_4 + M \rightarrow NO_2 + NO_3 + M$	$1.3 \times 10^{-5} \times \left(\dfrac{T_g}{298}\right)^{-3.8} \times \exp\left(-\dfrac{53210}{R_g T_g}\right)$	50	b, c
$N_2O_5 + M \rightarrow NO_2 + NO_3 + M$	$2.1 \times 10^{-11} \times \left(\dfrac{300}{T_g}\right)^{-3.5} \times \exp\left(-\dfrac{91460'}{R_g T_g}\right)$	45	b, c
$NO + O_2(g,v) + M \rightarrow NO_3 + M$	$5.65 \times 10^{-41} \times \exp\left(-\dfrac{1750}{R_g T_g}\right)$	61	a, b, c
$NO + O_2(E_x) + M \rightarrow NO_3 + M$	$5.65 \times 10^{-41} \times \exp\left(-\dfrac{1750}{R_g T_g}\right)$	61	b, d
$N + N + NO \rightarrow N_2(A^3\Sigma_u^+) + NO$	1.7×10^{-33}	45	
$N + N + NO \rightarrow N_2(B^3\Pi_g) + NO$	2.4×10^{-33}	45	
$N + N + O \rightarrow N_2(A^3\Sigma_u^+) + O$	1.0×10^{-32}	45	
$N + N + O \rightarrow N_2(B^3\Pi_g) + O$	1.4×10^{-32}	45	
$N + N + O_2 \rightarrow N_2(A^3\Sigma_u^+) + O_2$	1.7×10^{-33}	45	
$N + N + O_2 \rightarrow N_2(B^3\Pi_g) + O_2$	2.4×10^{-33}	45	
$N(2D) + N_2O \rightarrow NO + N_2$	3.5×10^{-12}	45	
$N(2D) + NO \rightarrow N_2 + O$	1.8×10^{-10}	45	
$N(2D) + O \rightarrow N + O(1D)$	4.0×10^{-13}	45	
$N(2D) + O_2(g,v) \rightarrow NO + O$	5.2×10^{-12}	45	a
$N(2P) + NO \rightarrow N_2(A^3\Sigma_u^+) + O$	3.0×10^{-11}	45	
$N(2P) + O \rightarrow N + O$	1.0×10^{-12}	45	
$N(2P) + O_2(g,v) \rightarrow NO + O$	2.6×10^{-15}	45	a
$N_2(a^3\Sigma_u) + NO \rightarrow N_2 + N + O$	3.6×10^{-10}	45	
$N_2(a^3\Sigma_u) + O \rightarrow NO + N$	3.0×10^{-10}	54	
$N_2(a^3\Sigma_u) + O_2(g,v) \rightarrow N_2 + O + O$	2.8×10^{-11}	45	a
$N_2(A^3\Sigma_u^+) + N_2O \rightarrow N_2 + N + NO$	1.0×10^{-11}	45	
$N_2(A^3\Sigma_u^+) + NO \rightarrow N_2 + NO$	6.9×10^{-11}	45	
$N_2(A^3\Sigma_u^+) + NO_2 \rightarrow N_2 + O + NO$	1.0×10^{-12}	45	
$N_2(A^3\Sigma_u^+) + O \rightarrow N_2 + O(1S)$	2.1×10^{-11}	45	
$N_2(A^3\Sigma_u^+) + O \rightarrow NO + N(2D)$	7.0×10^{-12}	45	
$N_2(A^3\Sigma_u^+) + O_2(g,v) \rightarrow N_2 + O + O$	$2.0 \times 10^{-12} \times \left(\dfrac{T_g}{300}\right)^{0.55}$	45	a
$N_2(A^3\Sigma_u^+) + O_2 \rightarrow N_2 + O_2(a^1\Delta)$	$2.0 \times 10^{-13} \times \left(\dfrac{T_g}{300}\right)^{0.55}$	45	
$N_2(A^3\Sigma_u^+) + O_2 \rightarrow N_2 + O_2$	2.54×10^{-12}	45	
$N_2(A^3\Sigma_u^+) + O_2(g,v) \rightarrow N_2O + O$	$2.0 \times 10^{-14} \times \left(\dfrac{T_g}{300}\right)^{0.55}$	45	a
$N_2(B^3\Pi_g) + N_2O \rightarrow N_2 + N + NO$	0.58×10^{-10}	62	
$N_2(B^3\Pi_g) + N_2O \rightarrow N_2 + N_2 + O$	0.58×10^{-10}	62	
$N_2(B^3\Pi_g) + O \rightarrow NO + N$	3.0×10^{-10}	54	
$N_2(C^3\Pi_u) + O \rightarrow NO + N$	3.0×10^{-10}	54	
$N_2(C^3\Pi_u) + O_2(g,v) \rightarrow N_2 + O + O$	3.0×10^{-10}	45	a
$NO + O_2(E_x) \rightarrow O + NO_2$	$2.8 \times 10^{-12} \times \exp\left(-\dfrac{23400}{T_g}\right)$	45	d, g

Reaction	Rate coefficient	Ref.	Notes
$NO_3 + O_2(E_x) \rightarrow O_3 + NO_2$	$1.5 \times 10^{-12} \times \exp\left(-\dfrac{15020}{T_g}\right)$	45	d, h
$O(1D) + N_2 \rightarrow N_2 + O$	2.3×10^{-11}	45	
$O(1S) + N \rightarrow O + N$	1.0×10^{-12}	45	
$O(1S) + N_2(g,v) \rightarrow O + N_2(g,v)$	1.0×10^{-17}	45	
$O_2(a^1\Delta) + N \rightarrow NO + O$	$2.0 \times 10^{-14} \times \exp\left(-\dfrac{600}{T_g}\right)$	45	
$O_2(a^1\Delta) + N_2(g,v) \rightarrow O_2 + N_2(g,v)$	3.0×10^{-21}	45	
$O_2(a^1\Delta) + NO \rightarrow O_2 + NO$	2.5×10^{-11}	45	
$O_2(b^1\Sigma^+) + N_2 \rightarrow O_2(a^1\Delta) + N_2$	$1.7 \times 10^{-15} \times \left(\dfrac{T_g}{300}\right)^{1.0}$	45	
$N_2(B^3\Pi_g) + NO \rightarrow N_2(A^3\Sigma_u^+) + NO$	2.4×10^{-10}	45	
$N_2(B^3\Pi_g) + O_2(g,v) \rightarrow N_2 + O + O$	3.0×10^{-10}	45	a

a For any species indicated with (g,v), g and v stand for its ground and vibrationally excited state, respectively.

b M represents any neutral species.

c $R_g = 8.3144598\,J.K^{-1}.mol^{-1}$ is the universal gas constant.

d $O_2(E_x)$ represents the two electronically excited states: $O_2(a^1\Delta)$ and $O_2(b^1\Sigma^+)$.

e The rate coefficient is assumed to be equal to the rate of $O + O_2 + M \rightarrow O_3 + M$.

f $O_2(A^3\Sigma^+, C^3\Delta, c^1\Sigma^-)$ is a combination of three electronic excited states at a threshold energy of 4.5 eV.
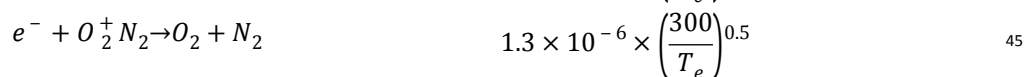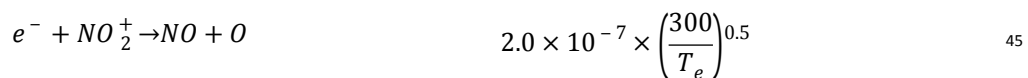
g The rate coefficient is assumed to be equal to the rate of $NO + O_2 \rightarrow O + NO_2$.

h The rate coefficient is assumed to be equal to the rate of $NO_3 + O_2 \rightarrow O_3 + NO_2$.

Tables S9 to S11 list the electron-ion recombination, the ion-neutral and the ion-ion reactions, and the corresponding rate coefficients, respectively. Table S12 displays the optical transitions.

Table S9. Electron-ion recombination reactions included in the model and the corresponding rate coefficient expressions. Te is to the electron temperature in K and Tg is the gas temperature in K.

Reaction	Rate coefficient	Ref.	Note
$e^- + N_2^+ \rightarrow N + N_{(g, E_x)}$	$R \times 1.8 \times 10^{-7} \times \left(\frac{300}{T_e}\right)^{0.39}$	45	a
$e^- + N_3^+ \rightarrow N_2 + N$	$2 \times 10^{-7} \times \left(\frac{300}{T_e}\right)^{0.5}$	63	
$e^- + N_3^+ \rightarrow N_2(E_x) + N$	$6.91 \times 10^{-8} \times \left(\frac{T_e}{11604.5}\right)^{-0.5}$	63	c
$e^- + N_4^+ \rightarrow N_2 + N_2$	$2.3 \times 10^{-6} \times \left(\frac{300}{T_e}\right)^{0.53}$	45	
$e^- + N_4^+ \rightarrow N_2 + N + N$	$3.13 \times 10^{-7} \times \left(\frac{T_e}{11604.5}\right)^{-0.41}$	63	
$e^- + N^+ + e^- \rightarrow e^- + N$	$7 \times 10^{-20} \times \left(\frac{300}{T_e}\right)^{4.5}$	63	
$e^- + N^+ + M \rightarrow N + M$	$6 \times 10^{-27} \times \left(\frac{300}{T_e}\right)^{1.5}$	64	b
$e^- + N_2^+ + e^- \rightarrow e^- + N_2$	$1 \times 10^{-19} \times \left(\frac{T_e}{300}\right)^{-4.5}$	63	
$e^- + N_2^+ + M \rightarrow N_2 + M$	$2.49 \times 10^{-29} \times \left(\frac{T_e}{11604.5}\right)^{-1.5}$	63	b
$e^- + O^+ + O_2 \rightarrow O + O_2$	$6 \times 10^{-27} \times \left(\frac{300}{T_e}\right)^{1.5}$	64	
$e^- + O^+ + e^- \rightarrow e^- + O$	$7 \cdot 10^{-20} \cdot \left(\frac{300}{T_e}\right)^{4.5}$	45	
$e + O_2^+ + M \rightarrow O_2 + M$	1×10^{-26}	37	b
$e^- + O_2^+ + e^- \rightarrow e^- + O_2$	$1 \times 10^{-19} \times \left(\frac{T_e}{300}\right)^{-4.5}$	64	
$e^- + O_2^+ \rightarrow O + O$	$6.46 \times 10^{-5} \times T_e^{-0.5} \times T_g^{-0.5}$	65	
$e^- + O_2^+ \rightarrow O + O(1D)$	$1.08 \times 10^{-7} \left(\frac{T_e}{300}\right)^{-0.7}$	45	
$e^- + O_2^+ \rightarrow O + O(1S)$	$0.14 \times 10^{-7} \left(\frac{T_e}{300}\right)^{-0.7}$	45	
$e^- + O_4^+ \rightarrow O_2 + O_2$	$1.4 \times 10^{-6} \times \left(\frac{300}{T_e}\right)^{0.5}$	45	
$e^- + NO^+ + e^- \rightarrow e^- + NO$	$1.0 \times 10^{-19} \left(\frac{T_e}{300}\right)^{-4.5}$	64	
$e^- + NO^+ + M \rightarrow NO + M$	$2.49 \times 10^{-29} \times \left(\frac{T_e}{11604.5}\right)^{-1.5}$	63	b
$e^- + NO^+ \rightarrow O + N(g,E_x)$	$R \times 4.2 \times 10^{-7} \times \left(\frac{300}{T_e}\right)^{0.85}$	45	d
$e^- + N_2O^+ \rightarrow N_2 + O$	$2.0 \times 10^{-7} \times \left(\frac{300}{T_e}\right)^{0.5}$	45	

| $e^- + NO_2^+ \rightarrow NO + O$ | $2.0 \times 10^{-7} \times \left(\dfrac{300}{T_e}\right)^{0.5}$ | [45] |
| $e^- + O_2^+ N_2 \rightarrow O_2 + N_2$ | $1.3 \times 10^{-6} \times \left(\dfrac{300}{T_e}\right)^{0.5}$ | [45] |

[a] In N(g, E_x), g stands for the ground state of atomic N and E_x represents two of its electronically excited states: $N(2D)$ and $N(2P)$; R is equal to 0.5, 0.45 and 0.05 for N, $N(2D)$ and $N(2P)$, respectively.

[b] M represents any neutral species.

[c] $N_2(E_x)$ represents $N_2(A^3\Sigma_u^+)$ and $N_2(B^3\Pi_g)$.

[d] In $N(g,E_x)$, g stands for the ground state of atomic N and E_x represents the electronic excited state $N(2D)$; R is equal to 0.2 and 0.8 for N and $N(2D)$, respectively.

Table S10. Ion-neutral reactions included in the model and the corresponding rate coefficient expressions. T_g is the gas temperature in K. For certain reactions, T_{ion} is the effective temperature of the reacting ion in K.[37]

Reaction	Rate coefficient	Ref.	Note
$N_2^+ + N \rightarrow N^+ + N_2$	$7.2 \times 10^{-13} \times \left(\frac{T_{ion}}{300}\right)$	45	
$N_2^+ + N + N_2 \rightarrow N_3^+ + N_2$	$9.0 \times 10^{-30} \times \left(\frac{400}{T_{ion}}\right)$	45	
$N_4^+ + N_2 \rightarrow N_2^+ + N_2 + N_2$	$2.1 \times 10^{-16} \times \left(\frac{Tion}{121}\right)$	45	
$N^+ + N_2 + N_2 \rightarrow N_3^+ + N_2$	$1.7 \times 10^{-29} \times \left(\frac{300}{Tion}\right)^{2.1}$	45	
$N_2^+ + N_2 + N_2 \rightarrow N_4^+ + N_2$	$5.2 \times 10^{-29} \times \left(\frac{300}{T_{ion}}\right)^{2.2}$	45	
$N' + N + N_2 \rightarrow N_2' + N_2$	1.0×10^{-29}	45	
$N' + N \rightarrow N_2'$	1.0×10^{-29}	66	
$N_3' + N \rightarrow N_2' + N_2$	6.6×10^{-11}	45	
$N_4' + N \rightarrow N' + N_2 + N_2$	1.0×10^{-11}	45	
$N_2' + N_2(A^3\Sigma_u') \rightarrow N_3' + N$	3.0×10^{-10}	44	
$O^- + M \rightarrow O + M + e^-$	4.0×10^{-12}	44	a
$O + O \rightarrow O_2 + e$	2.3×10^{-10}	67	
$O^- + O_2(g,v) + M \rightarrow O_3^- + M$	$1.1 \times 10^{-30} \times \exp\left(\frac{300}{T_g}\right)$	67	a, b
$O + O_2(g,v) \rightarrow O_3 + e$	5.0×10^{-15}	45	b
$O + O_3 \rightarrow O_2 + O_2 + e$	3.0×10^{-10}	68	
$O + O_3 \rightarrow O_3 + O$	5.3×10^{-10}	69	
$O' + O + M \rightarrow O_2' + M$	1.0×10^{-29}	64	a
$O^+ + O_2(g,v) \rightarrow O + O_2^+$	$1.9 \times 10^{-11} \times \left(\frac{T_g}{300}\right)^{-0.5}$	70	b
$O' + O_3 \rightarrow O_2' + O_2$	1.0×10^{-10}	64	
$O_2^- + M \rightarrow O_2 + M + e^-$	$2.7 \times 10^{-10} \times \left(\frac{T_g}{300}\right)^{0.5} \times \exp\left(-\frac{5590}{T_g}\right)$	70	a
$O_2 + O \rightarrow O_2 + O$	3.31×10^{-10}	67	
$O_2^- + O_2(g,v) + M \rightarrow O_4^- + M$	$3.5 \times 10^{-31} \times \left(\frac{T_g}{300}\right)^{-1.0}$	64,67,69	a, b
$O_2 + O_2 \rightarrow O_2 + O_2 + e$	2.18×10^{-18}	71	
$O_2 + O_3 \rightarrow O_3 + O_2$	4.0×10^{-10}	67	
$O_2^+ + O_2(g,v) + M \rightarrow O_4^+ + M$	$2.4 \times 10^{-30} \times \left(\frac{T_g}{300}\right)^{-3.2}$	64	a, b
$O_3 + M \rightarrow O_3 + M + e$	2.3×10^{-11}	70	a
$O_3 + O \rightarrow O_2 + O_2 + e$	1.0×10^{-13}	69	
$O_3 + O \rightarrow O_2 + O_2$	2.5×10^{-10}	36	
$O_3 + O \rightarrow O_3 + O$	1.0×10^{-13}	67	
$O_3 + O_3 \rightarrow O_2 + O_2 + O_2 + e$	3.0×10^{-10}	69	
$O_4 + O \rightarrow O + O_2 + O_2$	3.0×10^{-10}	64	
$O_4 + O \rightarrow O_3 + O_2$	4.0×10^{-10}	64	
$O_4^- + O_2 \rightarrow O_2^- + O_2 + O_2$	$1.0 \times 10^{-10} \times \exp\left(-\frac{1044}{T_g}\right)$	45	
$O_4' + O \rightarrow O_2' + O_3$	3.0×10^{-10}	64	
$O_4^+ + O_2 \rightarrow O_2^+ + O_2 + O_2$	$3.3 \times 10^{-6} \times \left(\frac{300}{T_g}\right)^{4.0} \times \exp\left(-\frac{5030}{T_g}\right)$	64	
$O^- + O_2(a^1\Delta) \rightarrow O_3 + e^-$	3.0×10^{-10}	45	

Reaction	Rate	Ref	Notes
$O_2 + O_2(a^+\Delta) \to O_2 + O_2 + e$	2.0×10^{-10}	45	
$O_2 + O_2(b^+\Sigma') \to O_2 + O_2 + e$	3.6×10^{-10}	45	
$O_2^+ + O_2(E_x) + M \to O_4^+ + M$	$2.4 \times 10^{-30} \times \left(\dfrac{T_g}{300}\right)^{-3.2}$	45	a, c, d
$O_4^+ + O_2(a^+\Delta) \to O_2^+ + O_2 + O_2$	1.0×10^{-10}	45	
$O_4^+ + O_2(E_x) \to O_2^+ + O_2 + O_2$	1.0×10^{-10}	45	c
$O^- + O_2(a^+\Delta) \to O_2^- + O$	1.0×10^{-10}	45	
$O^- + O_2(E_x) + M \to O_3^- + M$	$1.1 \times 10^{-30} \times \exp\left(\dfrac{300}{T_g}\right)$	45	a, c, e
$O_2^- + O_2(E_x) + M \to O_4^- + M$	$3.5 \times 10^{-31} \times \exp\left(\dfrac{T_g}{300}\right)^{-1.0}$	64	a, c, f
$N^+ + N + O_2 \to N_2^+ + O_2$	1.0×10^{-29}	45	
$N^+ + N_2O \to NO^+ + N_2$	5.5×10^{-10}	45	
$N^+ + NO \to N_2^+ + O$	3.0×10^{-12}	45	
$N^+ + NO \to NO^+ + N$	8.0×10^{-10}	45	
$N^+ + NO \to O^+ + N_2$	1.0×10^{-12}	45	
$N^+ + O + M \to NO^+ + M$	1.0×10^{-29}	45	a
$N^+ + O \to N + O^+$	1.0×10^{-12}	45	
$N^+ + O_2 \to NO^+ + O$	2.5×10^{-10}	45	
$N^+ + O_2 \to O^+ + NO$	2.8×10^{-11}	45	
$N^+ + O_2 \to O_2^+ + N$	2.8×10^{-10}	45	
$N^+ + O_3 \to NO^+ + O_2$	5.0×10^{-10}	45	
$N_2^+ + N_2O \to N_2O^+ + N_2$	5.0×10^{-10}	45	
$N_2^+ + N_2O \to NO^+ + N + N_2$	4.0×10^{-10}	45	
$N_2^+ + NO \to NO^+ + N_2$	3.3×10^{-10}	45	
$N_2^+ + O \to NO^+ + N$	$1.3 \times 10^{-10} \times \left(\dfrac{300}{T_{ion}}\right)^{0.5}$	45	
$N_2^+ + O_2 \to O_2^+ + N_2$	$6.0 \times 10^{-11} \times \left(\dfrac{300}{T_{ion}}\right)^{0.5}$	45	
$N_2^+ + O_3 \to O_2^+ + O + N_2$	1.0×10^{-10}	45	
$N_2O^- + N \to NO + N_2 + e^-$	5.0×10^{-10}	44	
$N_2O^- + O \to NO + NO + e^-$	1.5×10^{-10}	44	
$N_2O^+ + NO \to NO^+ + N_2O$	2.9×10^{-10}	45	
$N_3^+ + NO \to N_2O^+ + N_2$	7.0×10^{-11}	45	
$N_3^+ + NO \to NO^+ + N + N_2$	7.0×10^{-11}	45	
$N_3^+ + O_2 \to NO_2^+ + N_2$	4.4×10^{-11}	45	
$N_3^+ + O_2 \to O_2^+ + N + N_2$	2.3×10^{-11}	45	
$N_4^+ + NO \to NO^+ + N_2 + N_2$	4.0×10^{-10}	45	
$N_4^+ + O \to O^+ + N_2 + N_2$	2.5×10^{-10}	45	
$N_4^+ + O_2 \to O_2^+ + N_2 + N_2$	2.5×10^{-10}	45	
$NO^- + N_2O \to NO + N_2O + e^-$	$4.26 \times 10^{-10} \times \exp\left(-\dfrac{107.2}{T_g}\right)$	72	
$NO^- + NO \to NO + NO + e^-$	$3.28 \times 10^{-10} \times \exp\left(-\dfrac{105.1}{T_g}\right)$	72	
$NO^- + N \to N_2O + e^-$	5.0×10^{-10}	45	
$NO^- + N_2O \to NO_2^- + N_2$	2.8×10^{-14}	45	
$NO^- + NO_2 \to NO_2^- + NO$	7.4×10^{-10}	45	
$NO^- + O \to NO_2 + e^-$	1.5×10^{-10}	44	
$NO^- + O_2 \to O_2^- + NO$	5.0×10^{-10}	45	

Reaction	Rate	Ref	Note
$NO_2^- + N \rightarrow NO + NO + e^-$	5.0×10^{-10}	44	
$NO_2^- + N_2O_5 \rightarrow NO_3^- + NO_2 + NO_2$	7.0×10^{-10}	45	
$NO_2^- + NO_2 \rightarrow NO_3^- + NO$	4.0×10^{-12}	45	
$NO_2^- + NO_3 \rightarrow NO_3^- + NO_2$	5.0×10^{-10}	45	
$NO_2^- + O_3 \rightarrow NO_3^- + O_2$	1.8×10^{-11}	45	
$NO_2^+ + NO \rightarrow NO^+ + NO_2$	2.9×10^{-10}	45	
$NO_3^- + N \rightarrow NO + NO_2 + e^-$	5.0×10^{-10}	44	
$NO_3^- + NO \rightarrow NO_2^- + NO_2$	3.0×10^{-15}	45	
$NO_3^- + O \rightarrow NO + O_3 + e^-$	1.5×10^{-10}	44	
$O^- + N \rightarrow NO + e^-$	2.6×10^{-10}	45	
$O^- + N_2(g,v) \rightarrow N_2O + e^-$	0.5×10^{-13}	45	b
$O^- + N_2(A^3\Sigma_u^+) \rightarrow O + N_2 + e^-$	2.2×10^{-9}	45	
$O^- + N_2(B^3\Pi_g) \rightarrow O + N_2 + e^-$	1.9×10^{-9}	45	
$O^- + N_2O \rightarrow N_2O^- + O$	2.0×10^{-12}	45	
$O^- + N_2O \rightarrow NO^- + NO$	2.0×10^{-10}	45	
$O^- + NO + M \rightarrow NO_2^- + M$	1.0×10^{-29}	45	a
$O^- + NO \rightarrow NO_2 + e^-$	2.6×10^{-10}	45	
$O^- + NO_2 \rightarrow NO_2^- + O$	1.2×10^{-9}	45	
$O^+ + N + M \rightarrow NO^+ + M$	1.0×10^{-29}	45	a
$O^+ + N \rightarrow N^+ + O$	1.3×10^{-10}	45	
$O^+ + N_2(g,v) + M \rightarrow NO^+ + N + M$	$6.0 \times 10^{-29} \times \left(\frac{300}{T_{ion}}\right)^2$	45	a, b
$O^+ + N_2(g,v) \rightarrow NO^+ + N$	$\left(1.5 - 2.0 \times 10^{-3} \times T_{ion} + 9.6 \times 10^{-7} \times T_{ion}^2\right) \times 1.0 \times 1$	45	b
$O^+ + N_2O \rightarrow N_2O^+ + O$	2.2×10^{-10}	45	
$O^+ + N_2O \rightarrow NO^+ + NO$	2.3×10^{-10}	45	
$O^+ + N_2O \rightarrow O_2^+ + N_2$	2.0×10^{-11}	45	
$O^+ + NO \rightarrow NO^+ + O$	2.4×10^{-11}	45	
$O^+ + NO \rightarrow O_2^+ + N$	3.0×10^{-12}	45	
$O^+ + NO_2 \rightarrow NO_2^+ + O$	1.6×10^{-9}	45	
$O_2^- + N \rightarrow NO_2 + e^-$	5.0×10^{-10}	45	
$O_2^- + N_2(B^3\Pi_g) \rightarrow O_2 + N_2 + e^-$	2.5×10^{-9}	45	
$O_2^- + N_2(A^3\Sigma_u^+) \rightarrow O_2 + N_2 + e^-$	2.1×10^{-9}	45	
$O_3^- + N_2(B^3\Pi_g) \rightarrow O_3 + N_2 + e^-$	2.5×10^{-9}	44	
$O_3^- + N_2(A^3\Sigma_u^+) \rightarrow O_3 + N_2 + e^-$	2.1×10^{-9}	44	
$NO^- + N_2(B^3\Pi_g) \rightarrow NO + N_2 + e^-$	2.5×10^{-9}	44	
$NO^- + N_2(A^3\Sigma_u^+) \rightarrow NO + N_2 + e^-$	2.1×10^{-9}	44	
$N_2O^- + N_2(B^3\Pi_g) \rightarrow N_2O + N_2 + e$	2.5×10^{-9}	44	
$N_2O^- + N_2(A^3\Sigma_u^+) \rightarrow N_2O + N_2 + e$	2.1×10^{-9}	44	
$NO_2^- + N_2(B^3\Pi_g) \rightarrow NO_2 + N_2 + e^-$	2.5×10^{-9}	44	
$NO_2^- + N_2(A^3\Sigma_u^+) \rightarrow NO_2 + N_2 + e$	2.1×10^{-9}	44	
$NO_3^- + N_2(B^3\Pi_g) \rightarrow NO_3 + N_2 + e^-$	2.5×10^{-9}	44	
$NO_3^- + N_2(A^3\Sigma_u^+) \rightarrow NO_3 + N_2 + e$	2.1×10^{-9}	44	
$O_2^- + NO_2 \rightarrow NO_2^- + O_2$	7.0×10^{-10}	45	
$O_2^- + NO_3 \rightarrow NO_3^- + O_2$	5.0×10^{-10}	45	
$O_2^+ + N \rightarrow NO^+ + O$	1.2×10^{-10}	45	

Reaction	Rate coefficient	Ref.	Note
$O_2^+ + N_2(g,v) + N_2 \rightarrow O_2^+ N_2 + N_2$	$9.0 \times 10^{-31} \times \left(\dfrac{300}{T_{ion}}\right)^2$	45	b
$O_2^- + N_2(g,v) \rightarrow NO^+ + NO$	1.0×10^{-17}	45	b
$O_2^- + NO \rightarrow NO^+ + O_2$	6.3×10^{-10}	45	
$O_2^- + NO_2 \rightarrow NO^+ + O_3$	1.0×10^{-11}	45	
$O_2^- + NO_2 \rightarrow NO_2^- + O_2$	6.6×10^{-10}	45	
$O_2^+ N_2 + N_2 \rightarrow O_2^+ + N_2 + N_2$	$1.1 \times 10^{-6} \times \left(\dfrac{300}{T_{ion}}\right)^{5.3} \times \exp\left(-\dfrac{2360}{T_{ion}}\right)$	45	
$O_2^+ N_2 + O_2 \rightarrow O_4^+ + N_2$	1.0×10^{-9}	45	
$O_3^- + N \rightarrow NO + O_2 + e^-$	5.0×10^{-10}	44	
$O_3^- + NO \rightarrow NO_2^- + O_2$	2.6×10^{-12}	45	
$O_3^- + NO \rightarrow NO_3^- + O$	1.0×10^{-11}	45	
$O_3^- + NO_2 \rightarrow NO_2^- + O_3$	7.0×10^{-11}	45	
$O_3^- + NO_2 \rightarrow NO_3^- + O_2$	2.0×10^{-11}	45	
$O_3^- + NO_3 \rightarrow NO_3^- + O_3$	5.0×10^{-10}	45	
$O_4^- + N_2 \rightarrow O_2^- + O_2 + N_2$	$1 \times 10^{-10} \times \exp\left(-\dfrac{1044}{T_g}\right)$	45	
$O_4^- + NO \rightarrow NO_3^- + O_2$	2.5×10^{-10}	45	
$O_4^+ + N_2(g,v) \rightarrow O_2^+ N_2 + O_2$	$4.6 \times 10^{-12} \times \left(\dfrac{T_{ion}}{300}\right)^{2.5} \times \exp\left(-\dfrac{2650}{T_{ion}}\right)$	45	b
$O_4^+ + NO \rightarrow NO^+ + O_2 + O_2$	1.0×10^{-10}	45	

ᵃ M represents any neutral species.

ᵇ For any species indicated with (g,v), g and v stand for its ground and vibrationally excited state, respectively.

ᶜ $O_2(E_x)$ represents the electronically excited states: $O_2(a^1\Delta)$ and $O_2(b^1\Sigma^+)$.

ᵈ The rate coefficient is assumed to be equal to the rate of $O_2^+ + O_2 + M \rightarrow O_4^+ + M$.

e The rate coefficient is assumed to be equal to the rate of $O^- + O_2 + M \rightarrow O_3^- + M$.

ᶠ The rate coefficient is assumed to be equal to the rate of $O_2^- + O_2 + M \rightarrow O_4^- + M$.

Table S11. Ion-ion reactions included in the model, the corresponding rate coefficient expressions and the references. T_g is the gas temperature in K.

Reaction	Rate coefficient	Ref.	Note
$O^- + O^+ + M \rightarrow O_2 + M$	$1.0 \times 10^{-25} \times \left(\dfrac{300}{T_g}\right)^{2.5}$	70	a
$O^- + O_2^+ + M \rightarrow O_3 + M$	$1.0 \times 10^{-25} \times \left(\dfrac{300}{T_g}\right)^{2.5}$	70	a
$O_2^- + O^+ + M \rightarrow O_3 + M$	$1.0 \times 10^{-25} \times \left(\dfrac{300}{T_g}\right)^{2.5}$	70	a
$O_2^- + O_2^+ + M \rightarrow O_2 + O_2 + M$	$1.0 \times 10^{-25} \times \left(\dfrac{300}{T_g}\right)^{2.5}$	70	a
$O_3^- + O^+ + M \rightarrow O_3 + O + M$	$2.0 \times 10^{-25} \times \left(\dfrac{300}{T_g}\right)^{2.5}$	44	a
$O_3^- + O_2^+ + M \rightarrow O_3 + O_2 + M$	$2.0 \times 10^{-25} \times \left(\dfrac{300}{T_g}\right)^{2.5}$	44	a
$O^- + O_2^+ \rightarrow O + O + O$	$2.60 \times 10^{-8} \times \left(\dfrac{300}{T_g}\right)^{0.44}$	67	a
$O_3^- + O_2^+ \rightarrow O + O + O_3$	$1.0 \times 10^{-7} \times \left(\dfrac{300}{T_g}\right)^{0.5}$	67	a
$O^- + O^+ \rightarrow O + O$	$4.0 \times 10^{-8} \times \left(\dfrac{300}{T_g}\right)^{0.43}$	67	
$O^- + O_2^+ \rightarrow O_2 + O$	$2.6 \times 10^{-8} \times \left(\dfrac{300}{T_g}\right)^{0.44}$	67	
$O_2^- + O^+ \rightarrow O + O_2$	$2.7 \times 10^{-7} \times \left(\dfrac{300}{T_g}\right)^{0.5}$	67	
$O_2^- + O_2^+ \rightarrow O_2 + O_2$	$2.01 \times 10^{-7} \times \left(\dfrac{300}{T_g}\right)^{0.5}$	67	
$O_2^- + O_2^+ \rightarrow O_2 + O + O$	$1.01 \times 10^{-13} \times \left(\dfrac{300}{T_g}\right)^{0.5}$	67	
$O_3^- + O^+ \rightarrow O_3 + O$	$1.0 \times 10^{-7} \times \left(\dfrac{300}{T_g}\right)^{0.5}$	71	
$O_3^- + O_2^+ \rightarrow O_2 + O_3$	$2.0 \times 10^{-7} \times \left(\dfrac{300}{T_g}\right)^{0.5}$	67	
$NO^- + A^+ + M \rightarrow NO + A + M$	$2.0 \times 10^{-25} \times \left(\dfrac{300}{T_g}\right)^{2.5}$	44	a, b
$NO_2^- + A^+ + M \rightarrow NO_2 + A + M$	$2.0 \times 10^{-25} \times \left(\dfrac{300}{T_g}\right)^{2.5}$	44	a, b
$N_2O^- + A^+ + M \rightarrow N_2O + A + M$	$2.0 \times 10^{-25} \times \left(\dfrac{300}{T_g}\right)^{2.5}$	44	a, b
$NO_3^- + A^+ + M \rightarrow NO_3 + A + M$	$2.0 \times 10^{-25} \times \left(\dfrac{300}{T_g}\right)^{2.5}$	44	a, b
$O_3^- + B^+ + M \rightarrow O_3 + B + M$	$2.0 \times 10^{-25} \times \left(\dfrac{300}{T_g}\right)^{2.5}$	44	a, c

[a] M represents any neutral species.
[b] A represents N, O, N_2, O_2, NO, NO_2 and N_2O species.
[c] B represents N, N_2, NO, NO_2 and N_2O species.

Table S12. Optical transitions of N_2 and O_2 species. The rate coefficients are expressed in s^{-1}.

Reaction	Rate coefficient	Ref.	Note
$N_2(A^3\Sigma_u^+)\rightarrow N_2$	0.5	45	
$N_2(B^3\Pi_g)\rightarrow N_2(A^3\Sigma_u^+)$	1.35×10^5	45	
$N_2(a^1\Sigma_u^-)\rightarrow N_2$	1.0×10^2	45	
$N_2(C^3\Pi_u)\rightarrow N_2(B^3\Pi_g)$	2.45×10^7	45	
$O_2(a^1\Delta)\rightarrow O_2$	2.6×10^{-4}	45	
$O_2(b^1\Sigma^+)\rightarrow O_2$	8.5×10^{-2}	45	
$O_2(b^1\Sigma^+)\rightarrow O_2(a^1\Delta)$	1.5×10^{-3}	45	
$O_2(A^3\Sigma^+,C^3\Delta,c^1\Sigma^-)\rightarrow O_2$	11	45	a

$_a$ $O_2(A^3\Sigma^+, C^3\Delta, c^1\Sigma^-)$ is a combination of three electronic excited states at a threshold energy of 4.5 eV.

The reaction rate coefficient expressions of the vibrational-translational (VT) relaxations and vibrational-vibrational (VV) exchanges between N_2 - N_2, N_2 - O_2 and O_2 - O_2 are calculated using the Forced Harmonic Oscillator (FHO) model proposed by Adamovich et al.[73] This method offers a semi-classical non-perturbative analytical solution for VT and VV transitions of diatomic molecules, by averaging the VT and VV probabilities (P_{VT} and P_{VV}) over the one-dimensional Boltzmann distribution.

$$P_{VT}(i \rightarrow f) = \frac{(n_s)^s}{(s!)^2} \cdot \varepsilon^s \cdot exp\left(-\frac{2n_s}{s+1}\varepsilon\right) \tag{32}$$

$$P_{VV}(i_1, i_2 \rightarrow f_1, f_2) \simeq \frac{[n_s^{(1)} n_s^{(2)}]^s}{(s!)^2} \cdot \left(\frac{\rho_\varepsilon^2}{4}\right)^s \cdot exp\left[-\frac{2n_s^{(1)} n_s^{(2)} \rho_\varepsilon^2}{s+1}\frac{\rho_\varepsilon^2}{4}\right] \tag{33}$$

with $s = |i - f|$, $n_s = \left[\frac{\max(i,f)!}{\min(i,f)!}\right]^{1/s}$. ρ_ε and ε are collision and potential specific parameters.

Table S13. Vibrational – vibrational exchanges and vibrational – translational relaxations for N$_2$ (as an example) and the rate coefficient expression.
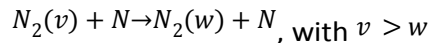
Reaction	Rate coefficient
$N_2(v_i) + M \rightarrow N_2(v_i - 1) + M$	$Z \cdot \left(\frac{m}{kT}\right)\int_0^\infty P_{VT}(\bar{v}) \cdot exp\left(\frac{-mv^2}{2kT}\right) v dv$
$N_2(v_i) + N_2(v_j) \rightarrow N_2(v_i - 1) + N_2(v_j + 1)$	$Z \cdot \left(\frac{m}{kT}\right)\int_0^\infty P_{VV}(\bar{v}) \cdot exp\left(\frac{-mv^2}{2kT}\right) v dv$

M represents any neutral particle in the plasma.
v_i and v_j are the vibrational levels of N_2 (0-24).
Z is the collision frequency and v is the particle velocity.

The reaction rate coefficients of the VT relaxations between N$_2$ – N are based on quasi classical calculations that have been reproduced through a fit as proposed by Esposito et al.,[74] for the following general reaction:

$$N_2(v) + N \rightarrow N_2(w) + N, \text{ with } v > w$$

All the relevant trends in the rate coefficients were taken into consideration by using an additive model into the exponential argument of the reaction rate coefficient, as shown in the following expression (valid for $v = 1 - 66$ and $\Delta v = 1 - 30$):

$$K(v, T, \Delta v) = exp\left(a_1(v,\Delta v) + \frac{a_2(v,\Delta v)}{T} + \frac{a_3(v,\Delta v)}{T^2} + \frac{a_4(v,\Delta v)}{T^3} + a_5(v,\Delta v) \cdot \ln(T)\right) \tag{34}$$

where

$$a_i(v, \Delta v) = z_{i0}(\Delta v) + z_{i1}(\Delta v)v + z_{i2}(\Delta v)v^2 + z_{i3}(\Delta v)v^3 + z_{i4}(\Delta v)v^4 \tag{35}$$

$$z_{ij}(\Delta v) = b_{ij} + c_{ij}\Delta v \tag{36}$$

For which the parameters are reported in Ref. [74]. Similarly, the reaction rate coefficients of the VT relaxations between $O_2 - O$ are based on quasi classical calculations that have been reproduced through a fit as proposed by Esposito et al.[75], for the following general reaction:

$$O_2(v) + O \rightarrow O_2(w) + O \text{, with } v > w$$
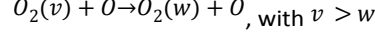
The reaction rate constant is then determined based on the following expression:

$$K(T, v, \Delta v) = DegF \cdot exp\left(a_1(v,\Delta v) + \frac{a_2(v,\Delta v)}{\ln(T)} + a_3(v,\Delta v) \cdot \ln(T)\right) \tag{37}$$

where Δv is $(v - w)$

$$a_i(v,\Delta v) = b_{i1}(\Delta v) + b_{i2}(\Delta v) \cdot \ln(v) + \frac{b_{i3}(\Delta v) + b_{i4}(\Delta v)v + b_{i5}(\Delta v)v^2}{10^{21} + \exp(v)} \tag{38}$$

$$b_{ij}(\Delta v) = c_{ij1} + c_{ij2} \cdot \ln(\Delta v) + c_{ij3} \cdot \Delta v \cdot \exp(-\Delta v) + c_{ij4} \cdot \Delta v \cdot \Delta v \tag{39}$$

The coefficients c_{ijk} have been generated using a linear least squares method and are reported in Ref. [75] where the degenary factor (DegF) is also explained.

S.13. Lumping the vibrational levels in the 2D non-thermal plasma model

To limit the calculation time in the 2D non-thermal model, we consider a reduced chemistry set in which the 24 vibrational levels of N_2 and the 15 vibrational levels of O_2 are each grouped together in one lumped vibrational level.[76] The lumping is achieved by summing the number density of all vibrational levels into the lumped level number density n_g:

$$n_g = \sum_{i=0}^{j} n_i \tag{40}$$

Here, n_i is the number density of the ith vibrational level (n_0 is considered the ground state number density). Note that j equals to 24 for N_2 and 15 for O_2.

To describe the distribution of the levels within the group, we assume a Boltzmann internal vibrational distribution giving:

$$n_i = \frac{n_g exp\left(-\frac{E_i}{k_b \cdot T}\right)}{\sum_{i=0}^{j} exp\left(-\frac{E_i}{k_b \cdot T}\right)} \tag{41}$$

where k_b is the Boltzmann constant, E_i is the energy of the ith level within the group, g, and T is the temperature associated to the group.

The conservation equation in the non-thermal plasma model is then solved for the lumped level density n_g:

$$\frac{\partial n_g}{\partial t} + \nabla(D\nabla n_g) + (\vec{u}_g \cdot \nabla)n_g = R_g \tag{42}$$

where D is the diffusion coefficient, $\vec{u}_g$ the gas flow velocity vector and R_g the sum of all production and loss rates, R_i, of each individual vibrational level due to chemical reactions:

$$R_g = \sum_{i=0}^{j} R_i \tag{43}$$

Additionally, the mean group vibrational energy conservation equation is required to describe the inner-distribution within the group.

$$\bar{E}_g = \frac{1}{n_g}\sum E_i n_i \tag{44}$$

We can then define a conservation equation for $\bar{E}_g$ by taking the time-derivative of Equation 44 and using Equation 43:

$$\frac{d\bar{E}_g}{dt} = \frac{\sum E_i R_i - \bar{E}_g \sum R_i}{n_g} \tag{45}$$

S.14. Drag force of the particle tracing simulations

The particle tracing simulations compute the trajectory of gas molecules through the reactor and report the "conditions" (i.e., gas temperature and power density) the molecules experience as a function of time, as they flow through the plasma towards the outlet. These trajectories are calculated using the particle tracing module in COMSOL, based on the drag force and velocity fields that were previously computed by the 3D turbulent gas flow model.

$$\frac{d(m_p v)}{dt} = F_D \tag{46}$$

This drag force F_D is calculated as follows:

$$\vec{F}_D = \frac{1}{\tau_p S}m_p(\vec{u}_g - \vec{v}_p) \tag{47}$$

In which m_p is the mass of the particle, $\vec{u}_g$ the velocity field calculated by the turbulent flow model and $\vec{v}_p$ the particle velocity, which differs from $\vec{u}_g$ due the inertia of the particles.
In Equation 47, τ_p and S are calculated using:

$$\tau_p = \frac{\rho_p d_p^2}{18\mu} \tag{48}$$

where ρ_p is the particle density, d_p the particle diameter and μ the dynamic viscosity of the fluid (see above).

$$S = 1 + K_n\left(C_1 + C_2 exp\left(-\frac{C_3}{K_n}\right)\right) \qquad (49)$$

In which K_n is a placeholder for following term:

$$K_n = \frac{\mu}{d_p}\sqrt{\frac{\pi}{2p\rho}} \qquad (50)$$

In which ρ and p are the gas density and gas pressure, respectively, as calculated by the turbulent flow model.

In Equation 49, C_1, C_2 and C_3 are the Cunningham-Millikan-Davies coefficients that consider the rarefaction with the following values:

C_1: 2.514
C_2: 0.8
C_3: 0.55

## S.15. Electron energy losses to various electron impact processes

Figure S3 shows the loss of the electron energy to the various possible electron impact collisions. The cross section set from the plasma kinetics model was used to calculate the electron energy loss coefficients with BOLSIG+[27] to which the gas composition of the feed gas is supplied, while taking into account a vibrational distribution. The energy loss fractions are calculated from a weighted summation according to the reacting molecules and the gas composition. Vibrational excitation (of N_2) is the main process occurring up till 70 Td. According to our modelling results, the reduced electric field in the RGA plasma ranges between 5 and 30 Td (i.e. 25-30 Td in the pulse and 0-5 in between the two pulses in the rotating arc and 15 Td in the steady arc). Therefore, vibrational excitation is the main process occurring in the RGA.
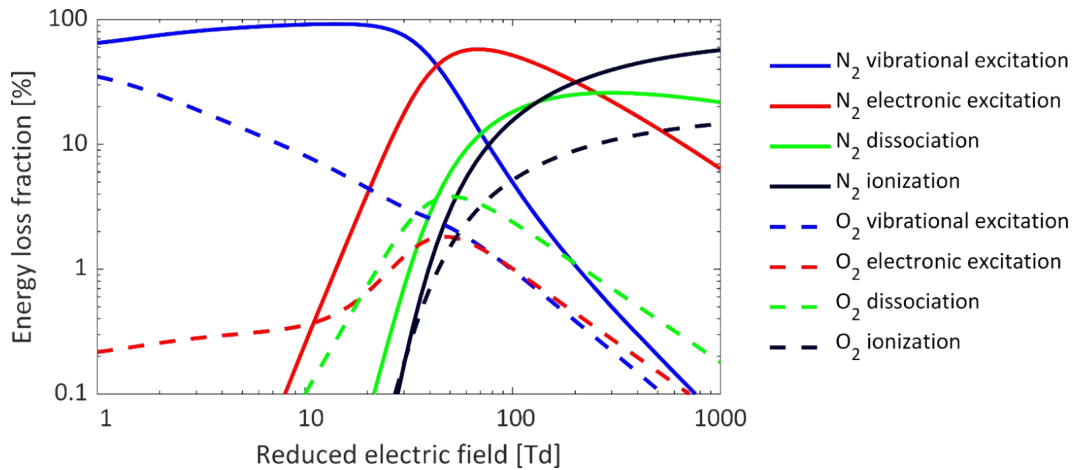
Figure S3. Electron energy losses to various electron impact processes (i.e. vibrational and electronic excitation, dissociation and ionization) as a function of the reduced electric field for a 80% N_2/20% O_2 feed gas and a plasma with both a gas temperature and vibrational temperature of 3000 K.

S.16. Path of particles in a rotating plasma arc

Particle tracing simulations illustrate the different paths followed by the gas molecules along their way through the reactor, where they experience different temperatures throughout their journey. Figure S4 shows the trajectories of the particles as well as the gas temperature, for the group experiencing a temperature between 2600 and 3000 K (indicated in black) and less than 2000 K (indicated in white). It is clear that the path of the particles that experience between 2600 and 3000 K flow through the hot centre of the arc where more reactive species are produced, resulting in higher NO_x production, as explained in the main text. Particles experiencing less than 2000 K don't flow through the hot centre of the arc or don't see the arc at all, resulting in a low NO_x production.
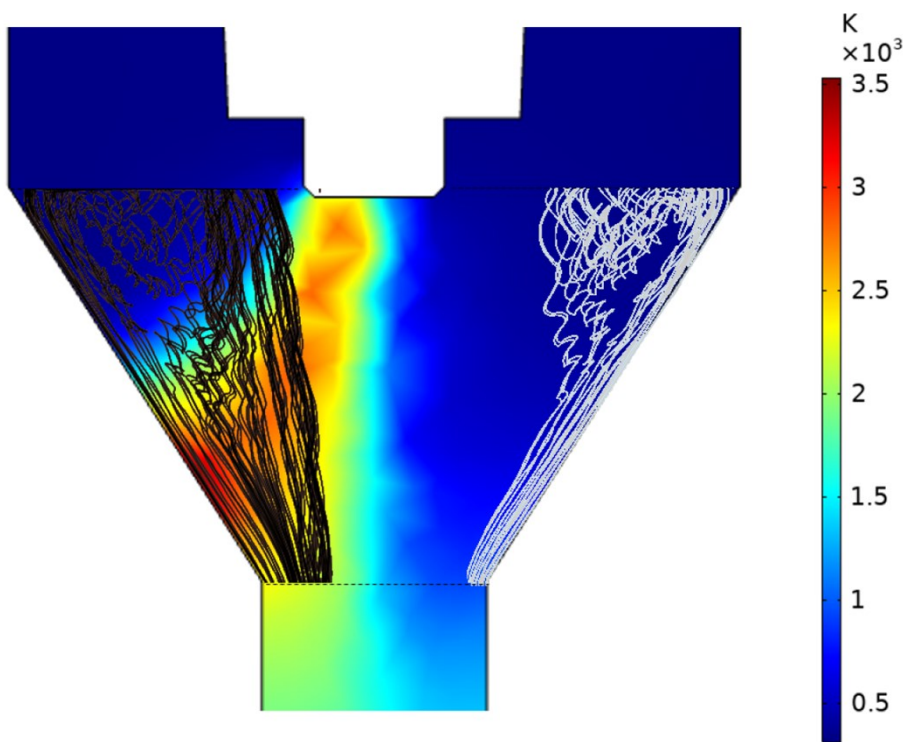
Figure S4. Calculated gas temperature distributions and the path of the gas molecules (indicated in black) experiencing gas temperature between 2600 and 3000 K (indicated in black) and less than 2000 K (indicated in white).

References:

1   Ammonia volatilization.

2   Y. Hou, G. L. Velthof and O. Oenema, *Glob. Chang. Biol.*, 2015, **21**, 1293–1312.

3   J. Clemens, S. Bergmann and R. Vandré, *Environ. Technol. (United Kingdom)*, 2002, **23**, 429–435.

4   K. Birkeland, *Trans. Faraday Soc.*, 1906, **2**, 98–116.

5   S. Eyde, *J. Ind. Eng. Chem.*, 1912, **4**, 771–774.

6   *Norsk Hydro testing 50kw pilot at Frognerkilen in 1903-1904. Telemark Museum Notodden*, .

7   W. S. Partridge, R. B. Parlin and B. J. Zwolinski, *Ind. Eng. Chem.*, 1954, **46**, 1468–1471.

8   M. Rahman and V. Cooray, *Opt. Laser Technol.*, 2003, **35**, 543–546.

9   W. Bian, X. Song, J. Shi and X. Yin, *J. Electrostat.*, 2012, **70**, 317–326.

10   R. D. Hill, I. Rahmim and R. G. Rinker, *1264 Ind. Eng. Chem. Res*, 1988, **27**, 1264–1269.

11   N. Rehbein and V. Cooray, *J. Electrostat.*, 2001, **51–52**, 333–339.

12   W. L. Chameides, D. H. Stedman, R. R. Dickerson, D. W. Rusch and R. J. Cicerone, *J. Atmos. Sci*, 1977, 143–149.

13   J. Li, S. Yao and Z. Wu, *J. Phys. D. Appl. Phys.*, 2020, **53**, 385201.

14   B. S. Patil, N. Cherkasov, J. Lang, A. O. Ibhadon, V. Hessel and Q. Wang, *Appl. Catal. B Environ.*, 2016, **194**, 123–133.

15   X. Pei, D. Gidon, Y. J. Yang, Z. Xiong and D. B. Graves, *Chem. Eng. J.*, 2019, **362**, 217–228.

16   X. Pei, D. Gidon and D. B. Graves, *J. Phys. D. Appl. Phys.*, 2020, **53**, 044002.

17   J. F. Coudert, B. J.M., J. Rakowitz and P. Fauchais, in *Proc. 3rd Int. Symp. on Plasma Chemistry*, 1977.

18   B. S. Patil, F. J. J. Peeters, G. J. van Rooij, J. A. Medrano, F. Gallucci, J. Lang, Q. Wang and V. Hessel, *AIChE J.*, 2018, **64**, 526–537.

19   W. Wang, B. Patil, S. Heijkers, V. Hessel and A. Bogaerts, *ChemSusChem*, 2017, **10**, 2110.

20   E. Vervloessem, M. Aghaei, J. F., N. Hafezkhiabani and A. Bogaerts, *ACS Sustain. Chem. Eng*, 2020, **8**, 9711–9720.

21   T. Kim, S. Song, J. Kim and R. Iwasaki, *Jpn. J. Appl. Phys.*, 2010, **49**, 126201.

22   B. Mutel, O. Dessaux and P. Goudmand, *Rev. Phys. Appliquée*, 1984, **19**, 461–464.

23   R. I. Asisov, V. K. Givotov, V. D. Rusanov and A. Fridman, *Sov. Phys., High Energy Chem.*, 1980, **14**, 366.

24   COMSOL Multiphysics.

25   F. R. Menter, M. Kuntz and R. Langtry, *Cfd.Spbstu.Ru*, 2003, **4**, 625–632.

26   L. C. P. S. Pancheshnyi, B. Eismann, G.J.M. Hagelaar, Computer code ZDPlaskin.

27   G. J. M. Hagelaar and L. C. Pitchford, *Plasma Sources Sci. Technol.*, 2005, **14**, 722–733.

28   V. Laporta, D. A. Little, R. Celiberto and J. Tennyson, *Plasma Sources Sci. Technol.*, 2014, **23**, 065002.

29   U. Eliasson, B.; Kogelschatz, *Basic Data for Modelling of Electrical Discharges in Gases: Oxygen*, Baden: ABB Asea Brown Boveri, 1986.

30   IST-Lisbon database, www.lxcat.net, retrieved in february 2018.

31   L. L. Alves, *J. phys. Conf. Ser.*, 2014, **656**, 1.

32   Morgan database, www.lxcat.net, retrieved in february 2018.

33   A. V. Lawton, S. A.; Phelps, Excitation of the b^1 sigma_g^+ state of O_2 by low energy electrons.

34   L. L. Alves, *J. phys. Conf. Ser.*

35   L. C. Phelps Database, www.lxcat.net, Phelps, A.V.; Pitchford, *Phys. Rev.*, 1985, **31**, 2932.

36   L. E. Khvorostovskaya and V. A. Yankovsky, *Contrib. to Plasma Phys.*, 1991, **31**, 71–88.

37   H. Hokazono, M. Obara, K. Midorikawa and H. Tashiro, *J. Appl. Phys.*, 1991, **69**, 6850–6868.

38   Itikawa database, www.lxcat.net, retrieved in february 2018.

39   Quantemol database, www.lxcat.net, retrieved in february 2018.

40   R. . C. J. Tennyson, V.; Laporta, *plasma sources sci. Technol.*, 2013, **22**, 025001.

41   Hayashi database, www.lxcat.net, retrieved in february 2018.

42   F. J. Gordillo-V'azquez, *J. Phys. D. Appl. Phys.*, 2008, **41**, 234016.

43   Y. Itikawa, *J. Phys. Chem. Ref. Data*, 2009, **38**, 1–20.

44   W. Wang, R. Snoeckx, X. Zhang, M. S. Cha and A. Bogaerts, *J. Phys. Chem. C*, 2018, **122**, 8704–8723.

45   Capitelli, *Plasma Kinetics in Atmospheric Gases*, Springer, 2000.

46   D. J. Kewley and H. G. Hornung, *Chem. Phys. Lett.*, 1974, **25**, 531–536.

47   M. A. A. . Clyne and D. H. Stedman, *J. Phys. Chem.*, 1967, **71**, 3071–3073.

48   W. Van Gaens and A. Bogaerts, *J. Phys. D. Appl. Phys.*, , DOI:10.1088/0022-3727/47/7/079502.

49   W. Tsang and R. F. Hampson, *J. Phys. Chem. Ref. Data*, 1986, **15**, 1087–1279.

50   R. Atkinson, D. L. Baulch, R. A. Cox, R. F. Hampson, J. A. Kerr Chairman and J. Troe, *J. Phys. Chem. Ref. Data*, 1997, **18**, 881–1097.

51   H. Hippler, R. Rahn and J. Troe, *J. Chem. Phys.*, 1990, **93**, 6560–6569.

52   J. M. Heimerl and T. P. Coffee, *Combust. Flame*, 1979, **35**, 117–123.

53   G. Suzzi Valli, R. Orrú, E. Clementi, A. Laganà and S. Crocchianti, *J. Chem. Phys.*, 1995, **102**, 2825–2832.

54   J. Baulch, D.L.; Cobos, C.J.; Cox, R.A.; Frank, P.; Hayman, G.; Just, Th.; Kerr, J.A.; Murrells, T.; Pilling, M.J.; Troe, J.; Walker, R.W.; Warnatz, *J. Phys. Chem. Ref. Data*, 1994, **23**, 847–1033.

55   J. Hjorth, *Int. J. Chem. Kinet.*, 1992, **24**, 51–65.

56   J. T. Herron, *J. Chem. Phys.*, 1961, **35**, 1138–1139.

57   P. P. Bemand, M. A. A. Clyne and R. T. Watson, *J. Chem. Soc. Faraday Trans. 2 Mol. Chem. Phys.*, 1974, **70**, 564–576.

58   R. Atkinson, D. L. Baulch, R. A. Cox, J. N. Crowley, R. F. Hampson, R. G. Hynes, M. E. Jenkin, M. J. Rossi, J. Troe, P. R. Center, L. H. Science, T. Centre and S. Park, *J. Phys. Chem. Ref. Data*, 2004, **I**, 1461–1738.

59   I. R. I. No, W. Tsang and J. T. Herron, .

60   H. S. Graham, R.A.; Johnston, *J. Phys. Chem.*

61   M. G. Ashmore, P.G.; Burnett, *J. Chem. Soc. Faraday Trans. 2*.

62   I. M. Campbell and B. A. Thrush, *Trans. Faraday Soc.*, 1966, **62**, 3366–3374.

63   W. L. Nighan, 1970, **2**, 1989–2000.

64   I. A. Kossyi, A. Y. Kostinsky, A. A. Matveyev and V. P. Silakov, *Plasma Sources Sci. Technol.*, 1992, **1**, 207–220.

65   R. E. Beverly, *Opt. Quantum Electron.*, 1982, **14**, 501–513.

66   R. Whitaker, M.; Biondi, M.A.; Johnsen, *Phys. Rev. A*, 1981, **24**, 743–745.

67   J. T. Gudmundsson and E. G. Thorsteinsson, *Plasma Sources Sci. Technol.*, 2007, **16**, 399–412.

68   A. A. Ionin, I. V. Kochetov, A. P. Napartovich and N. N. Yuryshev, *J. Phys. D. Appl. Phys.*, , DOI:10.1088/0022-3727/40/2/R01.

69   A. Cenian, A. Chernukho and V. Borodin, *Contrib. to Plasma Phys.*, 1995, **35**, 273–296.

70   T. G. Beuthe and J.-S. Chang, *Jpn. J. Appl. Phys.*, 1997, **36**, 4997–5002.

71   B. Eliasson, M. Hirth and U. Kogelschatz, *J. Phys. D. Appl. Phys.*, 1987, **20**, 1421–1437.

72   M. Mcfarland, D. B. Dunkin, F. C. Fehsenfeld, A. L. Schmeltekopf and E. E. Ferguson, *J. Chem. Phys.*, 1972, **56**, 2358–2364.

73   I. V. Adamovich, S. O. MacHeret, J. W. Rich and C. E. Treanor, *J. Thermophys. Heat Transf.*, 1998, **12**, 57–65.

74   F. Esposito, I. Armenise and M. Capitelli, *Chem. Phys.*, 2006, **331**, 1–8.

75   F. Esposito, I. Armenise, G. Capitta and M. Capitelli, *Chem. Phys.*, 2008, **351**, 91–98.

76   A. Berthelot and A. Bogaerts, *Plasma Sources Sci. Technol.*, 2016, **25**, 045022.